Journal of South American Earth Sciences 67 (2016) 122–139

Contents lists available at ScienceDirect

Journal of South American Earth Sciences

journal homepage: www.elsevier.com/locate/jsames

Petrology, geochemistry and thermobarometry of the northern area of the Flamenco pluton, Coastal Range batholith, northern Chile. A thermal approach to the emplacement processes in the Jurassic andean batholiths

Natalia Rodríguez [a], Juan Díaz-Alvarado [a, *], Carmen Rodríguez [b], Karl Riveros [a], Paulina Fuentes [a]

[a] Departamento de Geología, Universidad de Atacama, Copayapu 485, Copiapó, Chile
[b] Unidad Asociada de Petrología Experimental, CSIC-Universidad de Huelva, Campus El Carmen, 21071 Huelva, Spain

ARTICLE INFO

Article history:
Received 28 July 2015
Received in revised form
4 January 2016
Accepted 30 January 2016
Available online 23 February 2016

Keywords:
Thermal modeling
Contact aureole
Self-granulitization
Coast Range batholith
Northern Chile

ABSTRACT

The Flamenco pluton is part of a N–S alignment of Late Triassic to Early Jurassic intrusive belt comprising the westernmost part of the Coastal Range batholith in northern Chile. The Jurassic-Cretaceous voluminous magmatism related to subduction in the western active continental margin of Gondwana is emplaced in the predominantly metasedimentary Paleozoic host-rocks of the Las Tórtolas formation, which in the northern area of the Flamenco pluton present an intense deformation, including the Chañaral mélange.

Geochemically, the Flamenco pluton shows a wide compositional variability (SiO_2 between 48wt % and 67wt %). Gabbros, Qtz-diorites and tonalites, mesocratic and leucocratic granodiorites are classified as calc-alkaline, calcic, magnesian and metaluminous magmatism. Flamenco granitoids define cotectic linear evolution trends, typical of magmatic fractionation processes. Geochemical trends are consistent with magmas evolved from undersaturated and low-pressure melts, even though the absence of transitional contacts between intrusive units precludes in-situ fractionation. Although some granodioritic samples show crossed geochemical trends that point to the compositional field of metasediments, and large euhedral prismatic pinnite-biotite crystals, typical Crd pseudomorph, are observed in contact magmatic facies, geochemical assimilation processes are short range, and the occurrence of host-rocks xenoliths is limited to a few meters from the pluton contact.

A thermal approach to the emplacement process has been constrained through the thermobarometric results and a 2D thermo-numerical model of the contact aureole. Some Qtz-diorites and granodiorites located in the north area of the pluton exhibit granulitic textures as Hbl-Pl-Qtz triple junctions, poikiloblastic Kfs and Qtz recrystallization. The Hbl–Pl pairs have been used for the thermobarometric study of this metamorphic process, resulting granoblastic equilibrium temperatures between 770 and 790 °C, whereas Hbl–Pl pairs in domains that preserve the original igneous textures yield temperatures above 820 °C. This is characteristic of self-granulitization processes during the sequential emplacement of composite batholiths.

In addition, the thermal modeling was used in order to compare the expected and observed thermal contact aureole of the intrusive body. Model P-T conditions have been established between 3 and 4 kbars (extracted from the thermobarometric results), and temperatures between 1159 °C (*liquidus* temperature for a tonalitic composition) and 992 °C (fixed at the rheological threshold of a 50% crystal fraction). The thermal modeling estimates a homogeneous contact aureole, where the established temperatures for the melting reactions in the host-rocks are located at distances between 200 and 650 m from the magma chamber boundary, whereas the temperatures for Crd stabilization extend 1500 m far from the contact in the case of the emplacement at *liquidus* temperatures and 4 kbars. According to field observations, the contact aureole presents a scarce development in the northern area of the Flamenco pluton, with few

* Corresponding author.
E-mail address: juan.diaza@uda.cl (J. Díaz-Alvarado).

http://dx.doi.org/10.1016/j.jsames.2016.01.010

migmatite outcrops and less than 1 Km in thickness for Crd-schists. However, in the southern contact, partially melted rocks are described at distances up to 2 km from the Flamenco pluton boundary.

The processes of self-granulitization and the differences between the observed and calculated (by the thermal modeling of one single pulse) contact aureole suggests a process of incremental emplacement for the Flamenco pluton, by accretion of magmatic pulses from north to south (in its current position), where the thermal maturity reached through the repeated magmatic intrusion generates a more extensive area of high-grade metamorphism.

1. Introduction

The Flamenco pluton is part of the numerous and discontinuous outcrops of Late Paleozoic to Mesozoic igneous rocks emplaced in the Paleozoic metasedimentary basement which, taken together, form the so-called Coastal Range in northern Chile (Brook et al., 1986). Specifically, granitoids that make up the Flamenco intrusive body are framed in the voluminous calc-alkaline arc magmatism of Jurassic-Cretaceous age owing to the Coastal Range batholith. This magmatism was generated along the western Gondwana margin because of the reactivation of subduction in an extensional to transtensional tectonic regime in the Early Jurassic (Mpodozis and Kay, 1990; Dallmeyer et al., 1996; Grocott and Taylor, 2002).

The subduction in convergent margins has been proposed as the most efficient and sustainable mechanism to generate new continental crust since the Late Proterozoic (Kemp and Hawkesworth, 2003; Castro, 2014), supported by the statistical frequency of U–Pb zircon ages obtained from the continental crust (Condie, 1998, 2000). Cortical growth is directly related to the magmatism associated with subduction zones that are active without pronounced breaks, such as on the western margin of South America during the Andean cycle (Von Huene and Scholl, 1991 Plank and Langmuir, 1998). Therefore, subduction is the main engine for calc-alkaline magmatism and the formation of large cordilleran-type batholiths (Wyllie et al., 1976; Wyllie, 1977). Low water content, hybrid geochemical signatures and high compositional homogeneity are essential features for assessing the conditions and the sources of cordilleran magmatism (Castro, 2013; Burgisser and Bergantz, 2011). Several models have been proposed to generate these geochemical characteristics, such as the repeated intrusion of basaltic sills in a fertile lower crust (Annen y Sparks, 2002), the partial melting of crustal andesitic protoliths controlled by peritectic paragenesis ("PAE": peritectic assemblage entraintment) (Clemens et al., 2011, 2012), and the off-crust generation from partial melting of metasediment-MORB mélanges or cold diapirs that are finally relaminated to the continental crust and separated into residues (lower crust mafic granulites) and liquids (cordilleran magmatism) (Castro, 2013, 2014).

Re-thinking the emplacement and formation of large batholiths through geochronological data and detailed field and seismic studies (Glazner et al., 2004; Coleman et al., 2004) has outpaced old ideas about instantaneous balloon-like plutons (Bohrson and Spera, 2001; Huppert and Sparks, 1998). Although the batholith building is nowadays a controversial subject among the petrology community, many authors propose that incremental growth of composite batholiths is accomplished through small discrete magmatic pulses or batches (i. e., Annen, 2011; Michaut and Jaupart, 2011; Menand et al., 2015) over more than 10^5 years according to new and precise geochronological studies (i. e., Miller et al., 2007, 2011; Díaz-Alvarado et al., 2013), as has been confirmed by incorporating the influence of temperature on the crystallinity and thermal conductivity, and the depths of emplacement to the models (Gelman et al., 2013). The positive correlation between the period of amalgamation and the size of the batholith has highlighted that the availability of magmas in the crust depends on the fertility of both mantle and crust and the convergence dynamics between plates in convergent margins (Saint Blanquat et al., 2011). Thus, according to thermo-numerical models, magmatic addition rates in extensional arcs are higher than in continental margins with stable or compressive geodynamic regimes (Vogt et al., 2012). However, calculations for estimating the volumes of magma fluxes ascending to the upper crust are particularly difficult to determine. Although subduction is active during tens of millions of years, volumetrically, most of the magma is emplaced during periods of 10–30 Ma (Paterson et al., 2011).

Processes such as magma differentiation, fractionation, high-grade metamorphism and assimilation of host rocks may occur at the emplacement level, not only in the source area, and they are closely related to the style and emplacement rate of the magma chamber (Annen, 2011). Hence, variations in magma fluxes and the incubation period required to establish high-grade conditions account for the simultaneous presence in magmatic arcs of both magma–magma relations during the main intrusive phases and self-granulitization processes in earlier magmatic pulses (Annen and Sparks, 2002; Castro et al., 2014). The shape and thickness of the thermal aureole associated with a growing igneous body during the amalgamation of magma pulses depends on the emplacement constraints described above in addition to the thermal and mineralogical characteristics of the host rocks (Annen, 2011). Although the volume and the spatial distribution of magmatic increments rather than the shape of individual pulses determines the sequential growth of large batholiths (Paterson et al., 2011), most models propose small tabular bodies with horizontal disposition (i. e., Annen et al., 2006; Annen, 2011; Díaz-Alvarado et al., 2013). Accordingly, the development of the metamorphic aureole depends on the relative location of successive laminar pulses, and an irregular and non-concentric aureole would be formed during over-, under- or intra-accretion (Annen, 2011; Menand et al., 2010). Therefore, the formation of high-grade metamorphic areas in the host-rocks during the batholithic sequential emplacement depends on the temperatures and periodicity of intrusive magma fluxes and the location of crustal rocks in relation to the intrusive sheets; these are mostly related to crustal-scale tectonic structures that can increase and sustain high-grade and hyper-solidus conditions in the host rocks and residual liquids, respectively (Díaz-Alvarado et al., 2012, 2013; Annen, 2011).

The degree of development of the metamorphic aureole and tectonics influence the anisotropy and the disgregation of the host rock, a major control in the magnitude of the interaction processes between the intrusive magma and crustal rocks at the emplacement level. Mechanical mixing and reactive bulk assimilation account for considerable in-situ geochemical variations (i. e., Beard et al., 2005; Saito et al., 2007; Díaz Alvarado et al., 2011).

In this study, we present the first complete geochemical data from Flamenco pluton granitoids. Field relations, petrographic

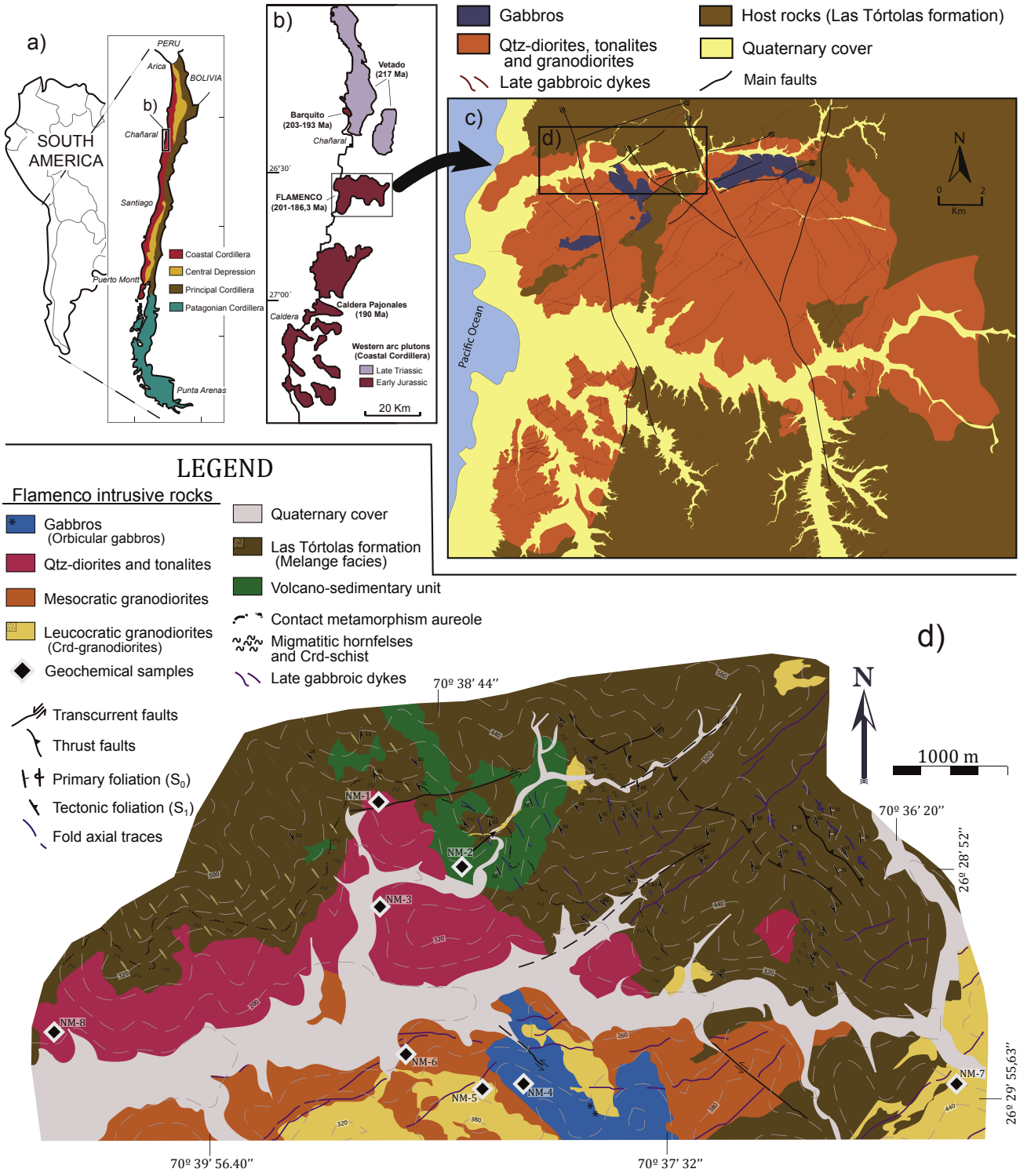

Fig. 1. (a) Major morphological features of the Andean cordillera in Chile (modified from Charrier et al., 2007). (b) Inset showing the outline of part of the Late Triassic-Early Jurassic Coastal Cordillera batholith. (c) Geological sketch of the entire Flamenco pluton based on field observations and satellite images. (d) Detailed geological map of the study area at the northwestern contact of the Flamenco pluton. The locations of the samples used in the geochemical study are indicated on the map.

features, geochemistry, thermobarometric data and thermal modeling allow us to determine the geochemical relations between the intrusive units and the extent of the interaction processes that occurred between intrusive magmas and metasedimentary host-rocks. In addition, we obtain a thermal setting to assess the batholith building processes during the emplacement of the Jurassic-Cretaceous magmas in northern Chile.

2. Geological setting

The geology of the Coastal Range batholith in northern Chile has been controlled by eastward subduction along the western margin

Fig. 2. Field photographs of some outstanding lithological and structural features of the study area. (a) Tonalites include irregular and partially digested xenoliths in areas near the contacts with metasedimentary host-rocks. (b) Self-thrusting of volcano-sedimentary layers showing previous boudinage and pinch and swell structures. (c) Sharp contacts between intrusive granodiorites and host Crd-Schists. (d) Elongated Crd crystals (black arrow) indicating the NW–SE syn-post-emplacement preferred orientation (red lines) of ductile structures in the contact aureole. (e) Orbicular textures found in gabbros from the study area. (f) Biotite-pinnite crystal clots (black arrows) showing euhedral prismatic shape and homogeneous grain size. (For interpretation of the references to color in this figure legend, the reader is referred to the web version of this article.)

of South American plate and global tectono-magmatic events since the Late Paleozoic. Following an almost total cessation of subduction during the Triassic-Early Jurassic rifting stage, the subsequent fragmentation of Gondwana caused a period of subduction reactivation and the earliest evidence of the magmatic arc development (~183 Ma), established in a crustal extensional context (Ramos, 1999; Charrier et al., 2007; Mpodozis and Ramos, 2008). During the NW–SE trending oblique convergence of the Phoenix and the South American plates, the high angle of subduction favored the negative velocity of trench roll-back (Mpodozis and Ramos, 2008). Thus, a magmatic arc was formed, located in the current coastal range (Fig. 1a, b).

Magmatic activity during the Triassic Pre-Andean cycle fits into a stationary period during the final consolidation of Pangea (Vilas and Valencio, 1978). This created a new tectonic context along the western margin of Gondwana that favored heat accumulation in the upper mantle and melting conditions in the lower crust, generating NNW-SSE trending elongated basins and large volumes of magma along the coast of northern Chile (Berg and Breitkreuz, 1983; Berg et al., 1983). In the study area, Late Permian magmatism is represented by granitic plutons called Quebrada del Castillo and Quebrada Quiscuda (264–244 Ma: Rb–Sr, Berg and Baumann, 1985; K–Ar, Ulriksen, 1979; K–Ar, Naranjo and Puig, 1984). Triassic intrusive magmas are leucocratic S-type granitoids, with $^{87}Sr/^{86}Sr$ between 0.7103 and 0.7172 (Berg y Baumann, 1985), and correspond to the plutons Pan de Azúcar (230 Ma: U–Pb, Berg and Baumann, 1985), Cerros del Vetado (217 Ma: U–Pb, Berg and Baumann, 1985) and Capitana (199–215 Ma: K–Ar and U–Pb, Godoy and Lara, 1998).

Subduction reactivation led to the formation of a Jurassic-Cretaceous magmatic arc, parallel to the west margin of Gondwana that has gradually migrated eastward and is located in the Principal Cordillera. This arc primarily forms the Coastal Cordillera batholith and is mostly composed of a calc-alkaline plutonic complex formed by hornblende-biotite gabbros, diorites, tonalites to granodiorites, and proportionally less granites (Dallmeyer et al.,

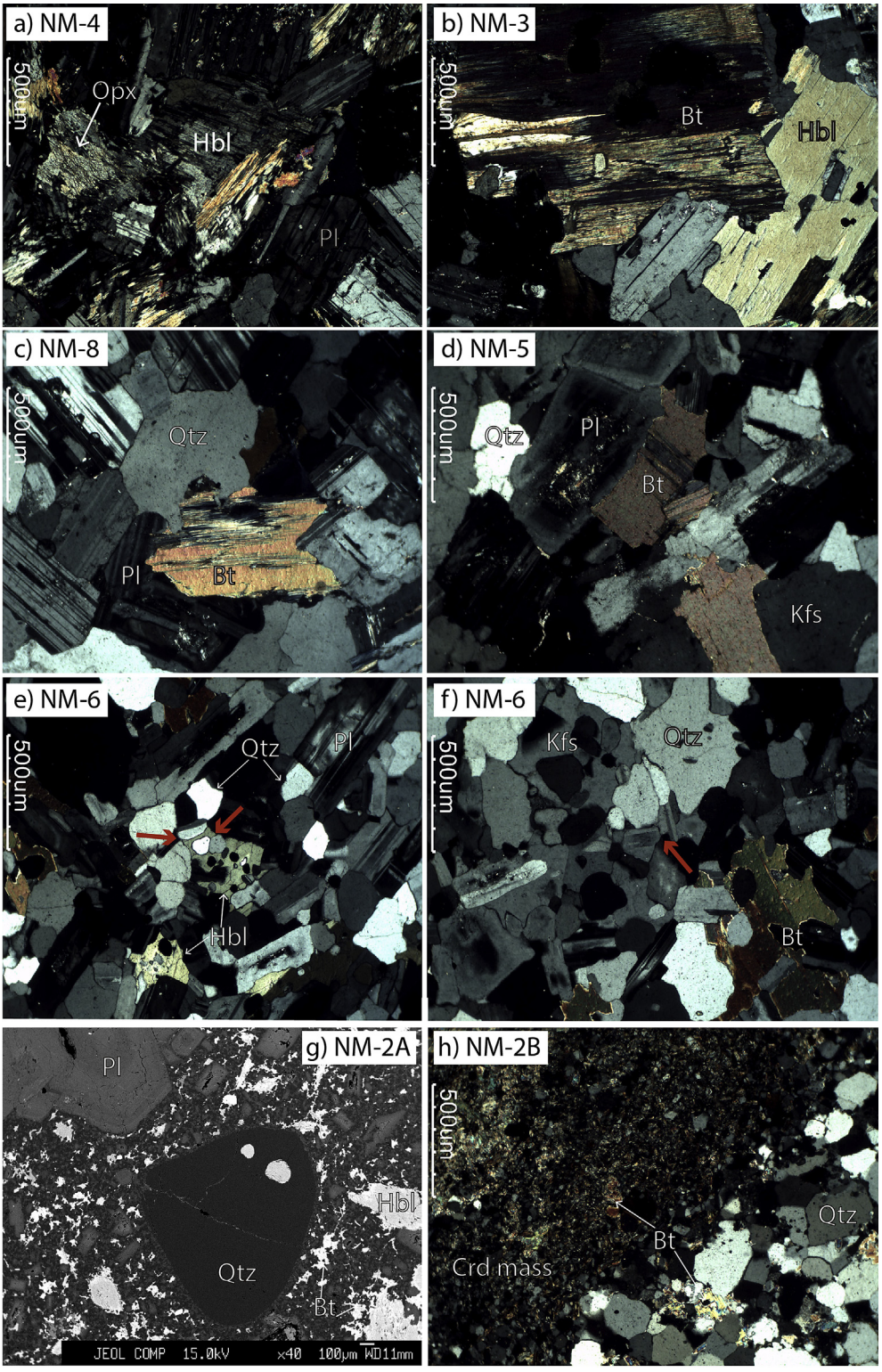

Fig. 3. Microphotographs showing the main petrographic characteristic of the studied samples. Most are cross-polarized light images except (g), which is a BSE image. Gabbros (a) present scarce Opx crystals, which are observed included in Hbl–Pl polycrystalline aggregates or clots derived from Px reaction in the melt. Qtz-diorites to granodiorites (b, c, d) show a progressive enrichment in Qtz and Kfs, and the substitution of Hbl by Bt as the mafic phase. Mesocratic granodiorites located at the north margin of Flamenco pluton (e, f) present granulitic recrystallization textures. Red arrows point to noteworthy examples of Hbl-Pl-Qtz triple junctions. Poikiloblastic Kfs and Qtz recrystallization are observed. Crd-granodiorites (g) show rounded and polycrystalline Qtz, and concentric zoned Pl and Hbl phenocrysts. Hbl present Bt reaction rims. The groundmass is composed of Qtz + Pl + Bt + Kfs. Crd-schists (h) present leucocratic Qtz-rich bands alternated with Crd-rich mesocratic domains. Some Qtz-rich bands show Kfs, incipient igneous textures and Bt-Crd schlierens, typical of migmatitic leucosomes. (For interpretation of the references to color in this figure legend, the reader is referred to the web version of this article.)

1996) in addition to andesitic, basaltic and dacitic volcanic rocks (González and Scheuber, 1997). Plutonic complexes were emplaced in Late Paleozoic metasedimentary basement rocks and Permian–Triassic plutonic complexes. Between 25°30′ S and 26°30′ S

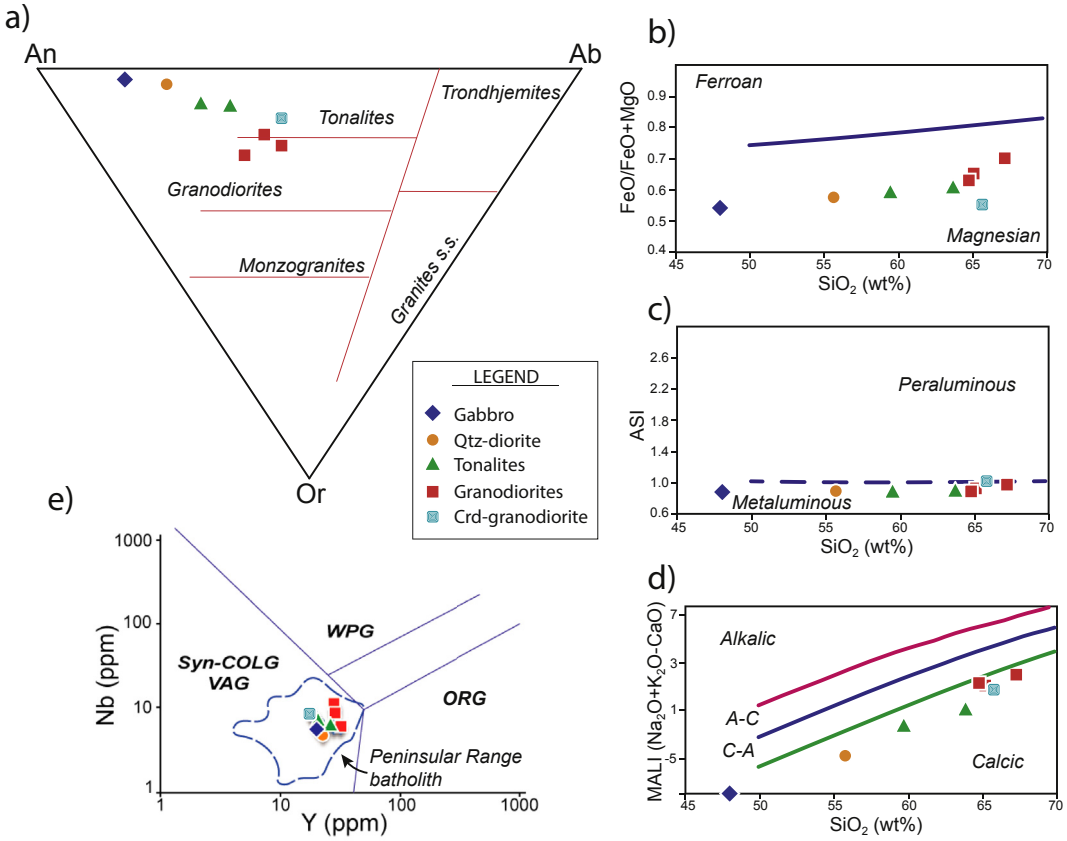

Fig. 4. (a) O'Connor rock classification triangle, (b, c, d) granitoid classification diagrams (Frost et al., 2001), and (e) Nb–Y tectonic discrimination diagram (Pearce et al., 1984) for the granitoids of the northern area of the Flamenco pluton. Only granodiorites show slight deviations from metaluminous and calcic trends defined by the Flamenco samples. In (e): WPG: Within-plate granite, ORG: Ocean ridge granite, VAR: Volcanic arc granite, Syn-COLG: Syn-collision granite.

(Fig. 1a, b), Jurassic plutons show a high compositional variability and correspond to the Bufadero and the Peralillo plutons (no data available), the Cerro Castillo (201.6 Ma: Rb–Sr, Berg y Baumann, 1985), the Barquito (193–204 Ma: K–Ar, Farrar et al., 1970; K–Ar, Díaz, 1986; Rb–Sr, Berg y Breitkreutz, 1983), the Las Ánimas (164–148 Ma: Rb–Sr, Berg y Breitkreutz, 1983; U–Pb, Berg y Breitkreutz, 1983; $^{40}Ar/^{39}Ar$, Dallmeyer et al., 1996; K–Ar, Díaz, 1986) and the Flamenco (described below) plutons. Volcanic rocks derived from the arc activity are found in the La Negra formation and the Punta del Cobre Group. These are basaltic to andesitic lavas interbedded with marine sedimentary rocks (Godoy and Lara, 1998). An extensional tectonic regime was maintained until the Late Cretaceous (Mpodozis y Ramos, 2008; Charrier et al., 2007).

The metasedimentary basement in the study area corresponds to the Las Tortolas formation, which has been defined as a turbiditic sedimentary succession developed at the shelf margin and talus environments (Bell, 1982). This formation comprises low to medium metamorphic grade mudstones and sandstones (mainly phyllites and quartzites) with minor limestones, conglomerates, volcanic rocks ("pillow" lavas) and pelagic cherts (Bell, 1982, 1987; Ulriksen, 1979; Naranjo and Puig, 1984; Godoy and Lara, 1998). The Las Tórtolas formation is included in the Chañaral Epimetamorphic Complex (CECh) (Godoy and Lara, 1998), forming two elongated NNE to SSW strips separated by a 100 km wide graben filled with younger sediments (Levi and Aguirre, 1981). Several depositional ages have been proposed for the turbidite rocks based on their fossil content, from Ordovician to Devonian (Bell, 1982; Naranjo and Puig, 1984), Carboniferous (Bahlburg et al., 1986), and Carboniferous to Permian (Bell, 1987).

The Las Tórtolas formation was tectonically deformed and subjected to greenschist facies metamorphism (Miller, 1970; Aguirre et al., 1972) during the Late Carboniferous or Early Permian. However, the formation includes an extremely deformed domain called Chañaral Melange that is defined as blocks of sandstone in a pelitic matrix (Bell, 1982, 1987). This deformation has been linked to a tectonic context of an accretionary wedge resulting from subduction towards the NE and the overlapping of several complex deformational events affecting unlithified sediments (Bell, 1987).

The Early Jurassic Flamenco pluton (Fig. 1c) intrudes the Las Tórtolas formation and corresponds to a sub-circular body of approximately 15 km in diameter comprising calc-alkaline Hbl-Bt tonalites to granodiorites, with minor Qtz-diorites and gabbros (Grocott et al., 1994), including orbicular gabbros (Godoy, 1997). The Flamenco pluton is intruded by conjugated sets of andesitic NW–SE and NE–SW dykes (Dallmeyer et al., 1996). The estimated ages for the pluton are between 201 and 186 Ma (Berg y Breitkreuz, 1983; Brook et al., 1986; Dallmeyer et al., 1996). The correlation between age and Hbl-blocking temperatures suggests magma emplacement in shallow cortical levels followed by rapid cooling (Dallmeyer et al., 1996).

3. Field relations and sample descriptions

The Flamenco pluton is emplaced in pelitic and quartzitic metasedimentary rocks of a highly deformed domain of the Las Tórtolas formation, which includes minor interbedded limestones and conglomerates (Fig. 1c). A meta-volcanosedimentary sequence outcrops at the northern contact of the Flamenco pluton (Fig. 1d). It is mainly comprised of basaltic and dacitic lavas with interbedded

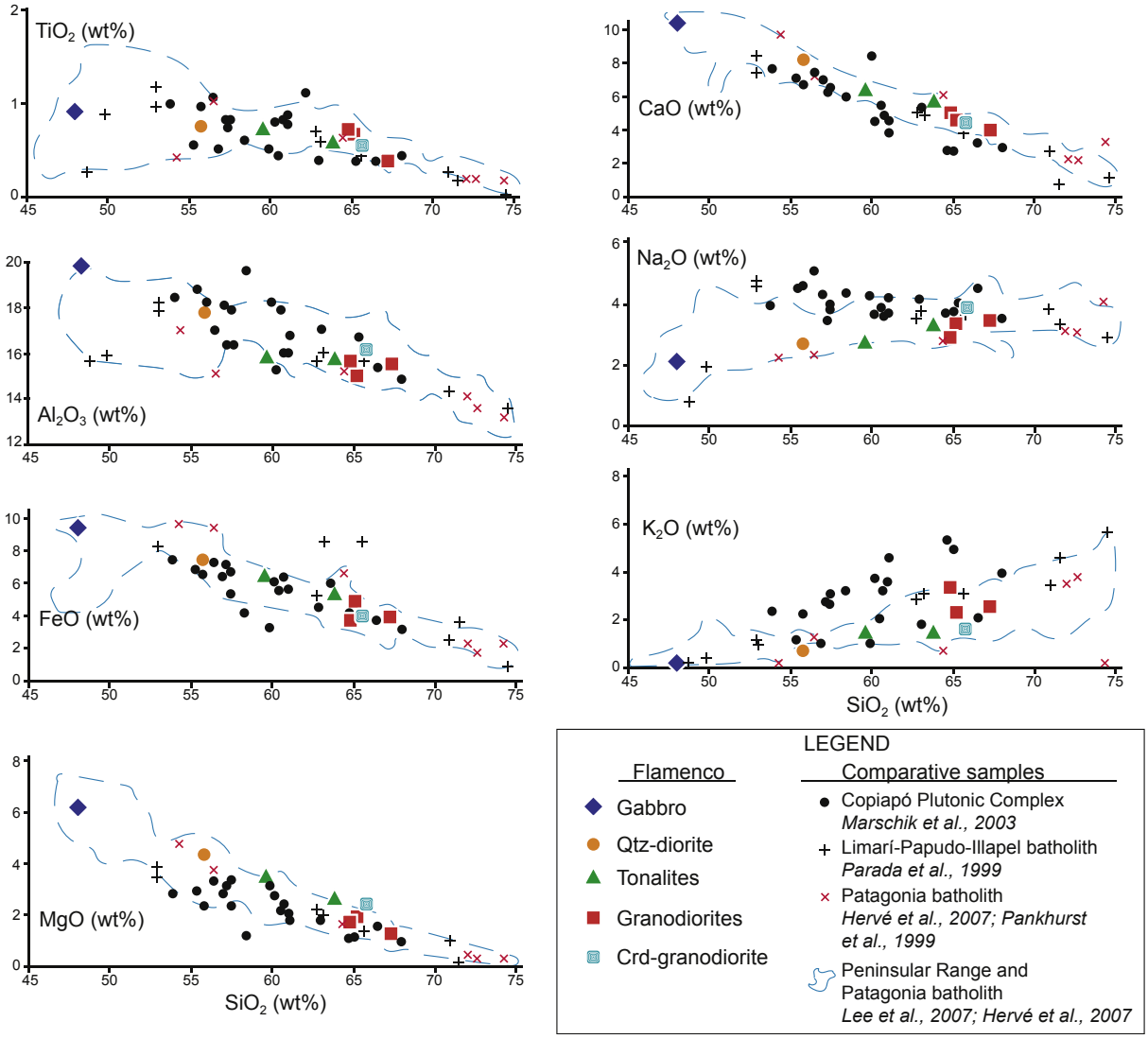

Fig. 5. Major element vs SiO_2 variation diagrams for the intrusive granitoids comprising the northern area of Flamenco pluton. The Copiapo Plutonic Complex (Marschik et al., 2003) and Limari-Papudo-Illapel batholith (Parada et al., 1999) are used as references for chronologically related plutonic rocks in the Coastal Cordillera batholith. Paradigmatic Cordilleran granitoids are plotted for comparison (Patagonia batholith: Hervé et al., 2007; Pankhurst et al., 1999; and Peninsular Range batholith: Lee et al., 2007).

quartzites and rare phyllites, and culminated at top with andesitic blocks and glass shards in a rhyolite mass. These rocks have not been previously described but are out of the scope of this study.

The north contact of the intrusive body has an irregular morphology with a W–E orientation and an approximately 18 km extension (Fig. 1d). According to satellite images and studies in other areas of the intrusive complex (i. e., Grocott and Taylor, 2002) (Fig. 1c), most of the contacts are sharp and steeply dipping. On a large scale, there are scarce kilometric fragments of host metasediment that are wholly or partially isolated within the intrusive granitoids (Fig. 1c). On a smaller scale, numerous metasedimentary irregularly shaped xenoliths of different sizes are hosted in the granitoids (Fig. 2a), always in the first few meters from the contact. Inland, only microgranular Qtz-dioritic enclaves are observed.

The Las Tórtolas formation shows three distinct domains in the study area according to their structural characteristics. The western area belongs to the melange facies (Fig. 1d), where the ellipsoidal quartzite objects included in a phyllite matrix show a primary NW–SE stretching lineation with low dips (between 5 and 20°). Foliations, where they can be measured, are NW–SE trending but SW and NE dipping. This is consistent with previous studies performed in the melange facies in other areas not directly influenced by the intrusive magmas (Bell, 1987). Melange textures are not present in the eastern area, but it features a strong deformation. Major structures are straight or slightly inclined SW vergent folds with N165E trending axial traces. Quartzites and some volcanic layers show boudinage and pinch and swell structures, which are further subjected to a second deformation phase causing autothrusting of the previously stretched or separate layers (Fig. 2b). In the eastern area, the structure is dominated by large lateral extension thrusts and associated propagation folds. These folds are verging to the SW and have identical axial traces defined by straight folds (Fig. 1d). Late transcurrent faults with N60E and N140E preferred orientations cut units and structures described above.

The contact aureole shows an irregular development in the metasedimentary formation in the north contact of the Flamenco pluton. Its thickness ranges from 50 to 800 m, dominated by Crd-schist (mineral abbreviations after Kretz, 1983) and to a lesser extent, migmatitic hornfelses with scarce leucosome bands or partial melting percentage (Fig. 2c). Migmatites are mainly developed in the pelitic lithologies, and from the contact into the metasedimentary formation, the metamorphic sequence is comprised

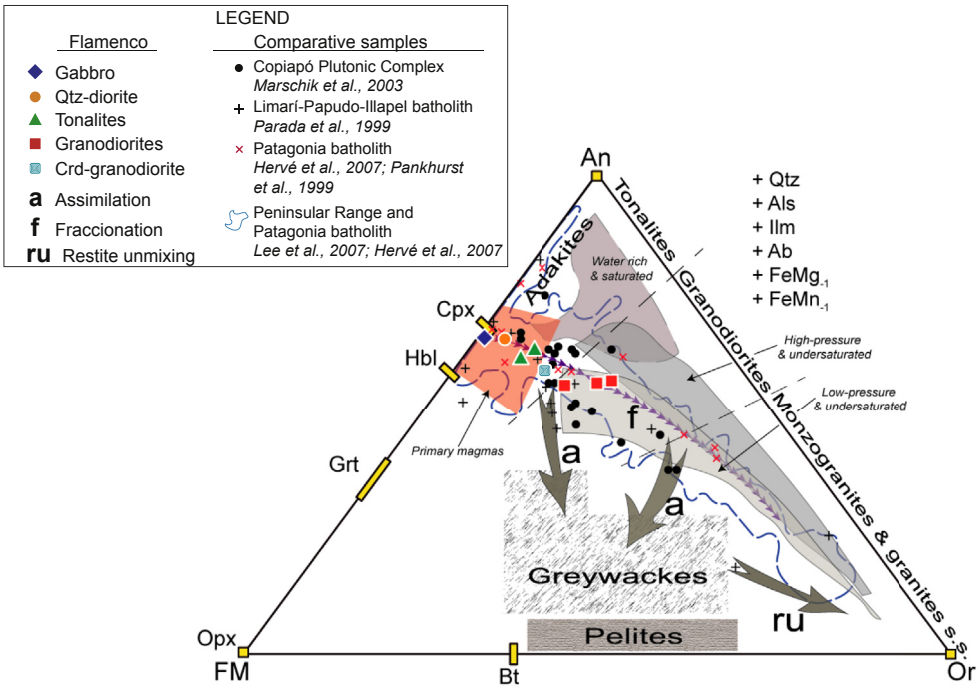

Fig. 6. Projection of the Flamenco granitoids into the F–An–Or projected space. Cotectic relations and crossed trayectories are evidenced in the pseudoternary system defined by Opx-An-Or. The main compositional areas and the experimental granitic evolutions are indicated (Díaz-Alvarado et al., 2011; Castro, 2013 and references therein). See text for further details.

by migmatitic hornfelses, Crd-schists and Crd-phyllites. In other areas of the contact aureole, this sequence is inverted (eastern part of the study area, Fig. 1d) where low-grade rocks (Crd-absent phyllites) are near the intrusive body, and the metamorphic grade increases toward the host rock. Changes in the metamorphic grade also appear to be tectonically controlled by NW–SE trending structures within the metasedimentary formation, resulting in strips of Crd-schist that progressively vary to low grade phyllites. Where Crd-schist attain a medium to large grain size, cordierites show a preferred orientation evidenced by a N150E trending plastic stretching lineation (Fig. 2d).

The Flamenco pluton shows large petrological variability in the study area, located in its northwest domain (Fig. 1b, c), which is representative of the entire pluton. The areas nearer the contact with the metasedimentary host rocks are dominated by Hbl Qtz-diorite to tonalite granitoids, and mesocratic granodiorites mostly outcrop toward the interior of the intrusive body. Several intrusive sheets of gabbros and leucocratic granodiorites are disposed in an approximate NNW-SSE orientation, presenting sharp contacts, self-enclaves and dykes in the host tonalites. Included in gabbroic facies, the presence of a small lensoidal shaped body of orbicular gabbros (Figs. 1d and 2e) is noteworthy. Several apophyses associated with the Flamenco pluton are isolated in the metasedimentary host rocks. The presence of an elongate dyke-like body of granodioritic composition that shows large idiomorphic prismatic crystals of biotite-pinnite (Fig. 2f) is notable. The main mineralogical and textural characteristics of the identified magmatic facies are listed below.

3.1. Petrographic descriptions

3.1.1. Gabbros (NM-4)

This unit is a fine-to medium-grained mesocratic rock that displays an isotropic fabric and phaneritic/hypidiomorphic textures. Its mineralogical composition is dominated by euhedral to subhedral, twinned and zoned Pl crystals (~65 vol.%) with a grain size of 0.75–2.5 mm that are weakly altered to sericite, calcite and epidote. Frequently, secondary Mg-rich Chl (~1 vol.%) fills the microfractures and the interstitial spaces developed in the Pl crystals. These rocks also contain subhedral to anehdral Hbl crystals (~35 vol.%) with a grain size of 0.6–5 mm that are moderately altered to Mg-rich Chl, whereas scarce secondary Bt (<1 vol.%) along the Hbl cleavage is also observed. Opx is present in the inner areas of Hbl aggregates (Fig. 3a). Opaque minerals and Qtz represent less than 2 vol.% of these rocks. A poikilitic texture is observed in the Hbl where it is enclosed by small Pl crystals.

3.1.2. Qtz-diorites (NM-3)

This unit is a medium-grained mesocratic rock showing an isotropic fabric and phaneritic/hypidiomorphic textures. Mineralogical composition of this rock unit is strongly dominated by euhedral to subhedral Pl (~60 vol.%) ranging from 0.25 to 3 mm, Hbl (~20 vol.%) with a grain size of 0.5–3.5 mm, Qtz (~7 vol.%) and Bt (~5 vol.%) showing grain sizes of 0.75–2 mm (Fig. 3b). Pl crystals are weakly altered to sericite and calcite, whereas Bt is strongly altered to Fe-rich Chl and moderately replaced by Ep. Subhedral Sph, Ap and opaque minerals represent the main accessory phases in these rocks. In concrete domains, corroded Opx grain boundaries and triple junctions between Hbl, Pl and Qtz are observed.

3.1.3. Tonalites (NM-1 and NM-8)

Tonalites consists of a fine-to medium-grained leucocratic rocks with an isotropic fabric and faneritic/equigranular texture (Fig. 3c). These rocks exhibit a wide range of alteration degree. Primary minerals in fresh tonalite include subhedral Pl (~55 vol.%) with a grain size of 0.5–1.5 mm, subheudral to anhedral Bt (~10 vol.%) with a grain size of 0.3–1.6 mm, subheudral to anhedral Hbl (2 vol.%) with a grain size of 0.5–2.75 mm, and anhedral Qtz (~25 vol.%). Accessory minerals are represented by sphene and opaque minerals.

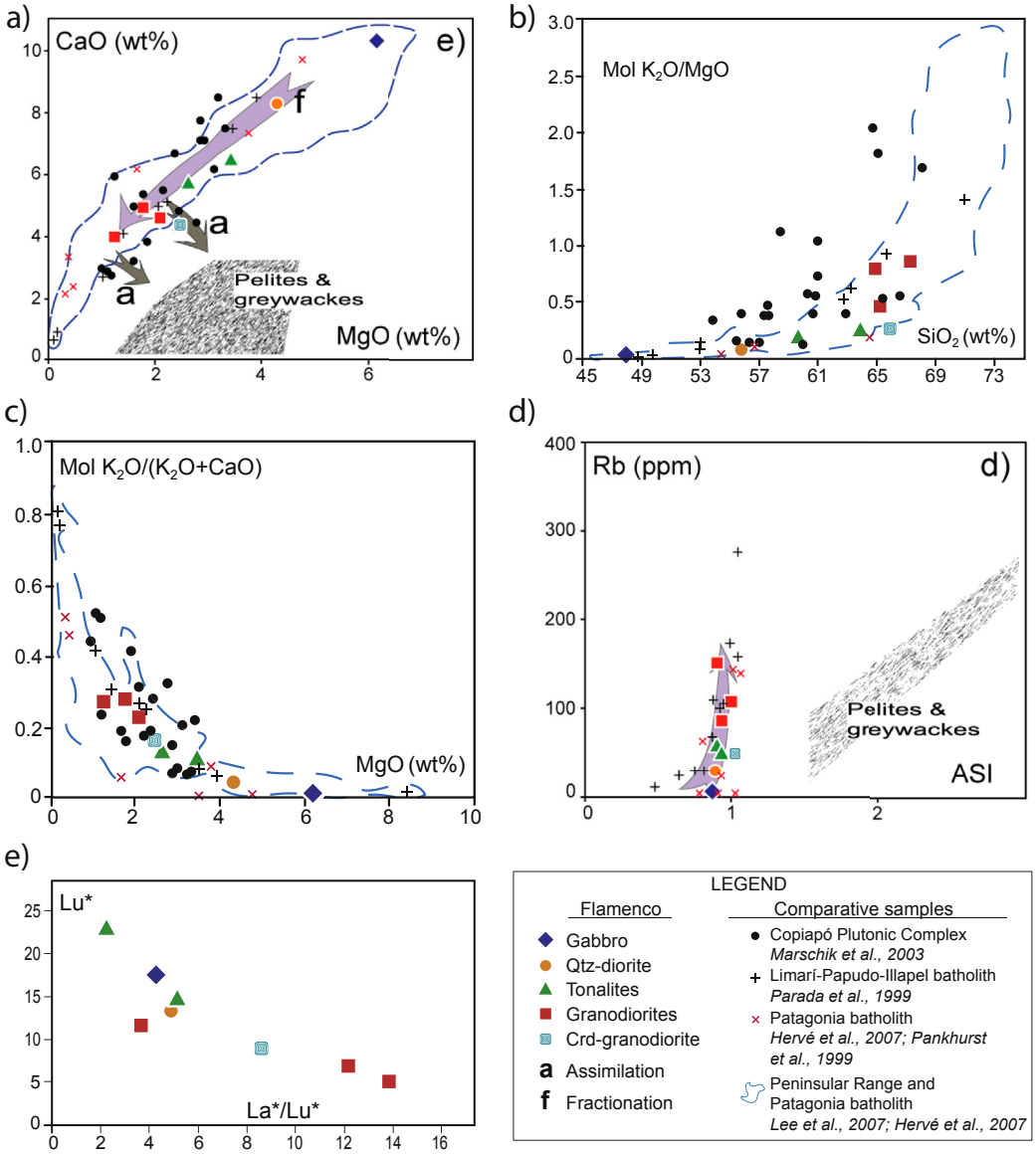

Fig. 7. Major and trace element geochemical variations. (a, b, c, d) Fractionation, cotectic-like and assimilation trends are indicated. Assimilation trajectories point to the host graywackes and pelites, showing Al_2O_3, FeO and MgO enrichment during CaO depletion. (e) Lu* vs La*/Lu* ratio. Low HREE values for granodiorites indicate the presence of Hbl during fractionation.

3.1.4. Leucocratic granodiorites (NM-5 and NM-7)

Rocks from this unit exhibit a fine-grained hypidiomorphic, equigranular and phaneritic textures in which the mineralogical composition is dominated by subhedral Pl crystals (~50 vol.%), that are between 0.5 and 1.75 mm, anhedral Qtz (~25 vol.%) with crystals smaller than 1.5 mm, subhedral Kfs (~10 vol.%) ranging from 0.25 to 1.5 mm and anhedral to subhedral Bt (~7 vol.%) with a grain size of 0.5–1.7 mm (Fig. 3d). The main accessory phases in these rocks are represented by euhedral to subheudral Sph that have crystals smaller than 1 mm and anhedral opaque minerals smaller than 0.25 mm.

3.1.5. Mesocratic granodiorites (NM-6)

Mesocratic granodiorites show two main textural domains. Where igneous textures are present, they present an isotropic fabric and equigranular, hypidiomorphic and fine-grained phaneritic textures. However, granoblastic textures are dominant over wide areas, where Hbl-Pl-Qtz triple junctions (Fig. 3e), poikiloblastic Kfs (Fig. 3f) and an extensive recrystallization are observed (Fig. 3e, f). The mineralogical composition is dominated by subhedral and twinned Pl (~45 vol.%) with crystals smaller than 1.5 mm, anhedral Qtz (~35 vol.%) with a grain size of 0.15–0.5 mm, subhedral Bt (~10 vol.%) ranging from 0.25 to 1.25 mm, subheudral Hbl (~5 vol.%) with a grain size of 0.25–2.5 mm and subheudral Kfs (~2–3 vol.%) showing a grain size of 0.25–1.5 mm. Scarce and small opaque crystals represent the main accessory phases in these rocks.

3.1.6. Crd-granodiorites (NM-2A)

This unit exhibits a distinctive glomeroporphyritic texture with medium-grained phenocrysts and xenocrysts (smaller than 7 mm) that represent approximately 55 vol. % of these rocks (Fig. 3g). These medium size crystals comprise subheudral to anhedral zoned and twinned Pl (~35 vol.%), polycrystalline rounded Qtz xenocrysts (~10 vol.%) (Fig. 3g), Kfs (~5 vol.%), Hbl (~3 vol.%) and Bt (~2 vol.%). Phenocrysts of Hbl are moderately to strongly affected by secondary and fine-grained biotite. Clots of fine-grained Bt, Kfs and quartz

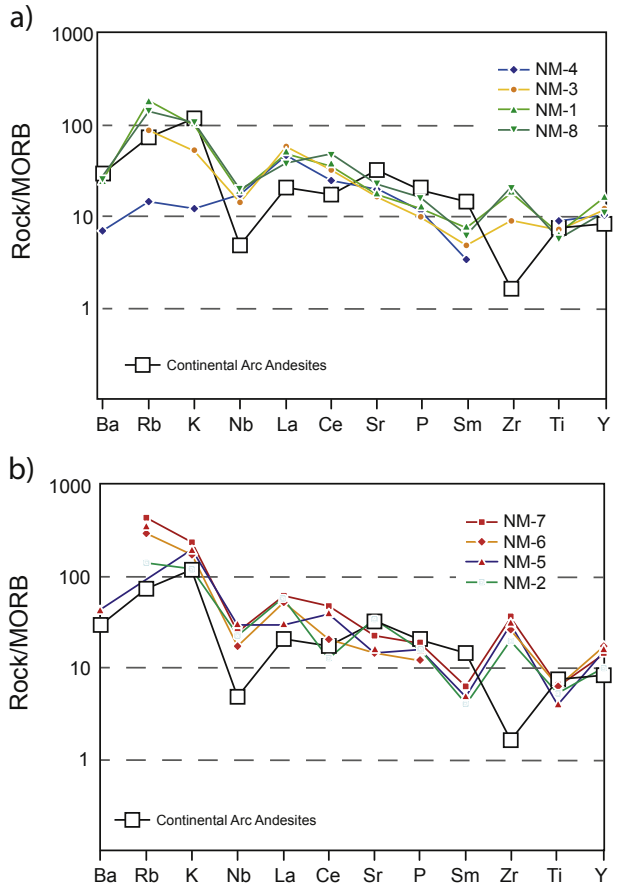

Fig. 8. Thompson normalization plot rock/MORB for (a) gabbros, Qtz-diorites and tonalites, and (b) granodiorites. The black line with white squares is the typical continental arc andesite composition given by Kelemen et al. (2003).

occur within prismatic and subhedral Bt phenocrysts, which mostly show hexagonal sections. The groundmass (~45 vol.%) shows crystals smaller than 0.25 mm and is completely obliterated by a secondary fine-grained assemblage of Qtz-Pl (~30 vol.%) and Bt (~10 vol.%), whereas Kfs crystals (~5 vol.%) also occur. The main accessory phases are related to zircon and opaque minerals.

3.1.7. Crd-schists (NM-2B)

Crd-schists are the most representive facies in the metasedimentary host-rocks. They are characterized by a granolepidoblastic texture related to a millimetric alternance of quartz-rich (leucocratic) and mica-rich (mesocratic) continuous to discontinuous bands. The limits of these mineralogical bands are sinuous, sharp and well-defined (Fig. 3h). Leucocratic bands mainly comprise anhedral Qtz crystals (~90–95 vol.%) ranging from 0.025 to 0.5 mm and minor amounts of fine anhedral to subhedral Ms and Bt (~5–10 vol.%), with a grain size smaller than 0.25 mm. The mesocratic bands are dominated by a mix of subhedral fine-grained Bt (~60 vol.%), anhedral Qtz (~10 vol.%) and anhedral Crd (~30 vol.%), in which most of the crystals are smaller than 0.05 mm. Bt crystals display an incipient orientation. Opaque minerals (~2–3 vol.%) show an average grain size of 0.025 mm and occur only in the mesosome bands.

4. Geochemistry

4.1. Sampling and analytical techniques

Selected samples for the geochemical study of the Flamenco pluton were collected along the northern contact of the intrusive body with metasedimentary rocks of the Las Tórtolas formation (Fig. 1d). Eight samples were chosen for major and trace element analyses to characterize the main facies composing the pluton in the study area. Geochemical data have been plotted to determine their geochemical and genetic relationships and to point some clues about the magmatic processes involved during the generation, ascent and emplacement of the magmas. Additionally, the selection of sampling points, with different spatial and textural relationship with the host rocks (presence of enclaves or exotic mineralogies) allows us to assess the extent of the processes of interaction between the intrusive magmas and the metasedimentary rocks at the emplacement level. The geochemical data of the studied samples are presented in Figs. 4–8 and in Table 1. For comparative data, two plutonic complexes of the Coastal Range Batholith were used. The Lower Cretaceous Copiapó Plutonic Complex (Marschik et al., 2003) and the Lower Jurassic to Lower Cretaceous Limari-Papudo-Illapel batholith (Parada et al., 1999) were selected because of their spatial and geochronological relationship with the Flamenco pluton, and the scarcity of geochemical data along the Coastal Range batholith. Additionally, two referenced examples of cordilleran batholiths are projected in variation diagrams (Patagonia batholith: Hervé et al., 2007; Pankhurst et al., 1999; and Peninsular Range batholith: Lee et al., 2007).

Approximately 3 kg of fresh rock was collected from each outcrop. Samples were crushed and milled to a fine powder in steel cups. Major elements were analyzed by X-ray fluorescence (XRF), with a Siemens SRS-3000 at the Universidad Católica del Norte (Chile). The precision of the XRF technique is between 0.1% and 1%. Trace elements, including rare earth elements (REE), were analyzed by inductively coupled plasma atomic emission spectrometry (ICP-AES) with a Perkin–Elmer Optima 2000 DV model at the Universidad Católica del Norte (Chile). The sample is dissolved in a Claisse M4 Fluxer with a Na_2CO_3–$Li_2B_4O_7$ mixture. This residue is dissolved in approximately 4 ml of HNO_3 and distilled water, and the solution is passed through a fractionation column containing an ion exchange resin (Dowex 50-WX8) separating the REEs, which are then eluted with 50 ml of HNO_3 6 N and 20 ml HNO_3 8 N. To achieve accuracy and precision with the method, two international standards (GA and GH) from Centre National de la Recherche Scientifique (CNRS, France) are used.

4.2. Geochemistry results

The Flamenco granitoids present a high percentage of CaO with respect to alkalis (Fig. 4a), showing an almost linear trend from gabbros to tonalites and granodiorites. Together, the samples describe a magnesian, metaluminous and calcium magmatic series (Fig. 4b, c, d). Both ASI vs. SiO_2 and MALI diagrams (Fig. 4c, d) (Frost et al., 2001) show that the most SiO_2 rich samples point to peraluminous and calc-alkalic fields, respectively, denoting alkali and alumina enrichment for the most evolved terms (Fig. 4b, c, d). According to the Nb vs. Y tectonic discrimination diagram (Fig. 4e) (Pearce et al., 1984), Flamenco granitoids belong to syn-collisional volcanic arc granitoids.

Harker diagrams show mainly linear trends for the magmatic facies that form the north area of the Flamenco pluton, with a wide SiO_2 range (48–67%) from gabbros to granodiorites (Fig. 5). TiO_2, Al_2O_3, MgO, FeO y CaO describe negative trends versus silica, whereas K_2O increases and Na_2O shows a flat or slightly positive pattern. Nevertheless, granodiorites display a more scattered distribution for some elements (K_2O, Na_2O and Al_2O_3, Fig. 5). The studied samples match the compositional trends drawn by typical calc-alkaline cordilleran batholiths. Only the Copiapó Plutonic Complex shows a different geochemical pattern, indicating the

Table 1
Whole-rock analyses of major and trace elements of granitoids of the northern area of the Flamenco pluton.

Rock type	Tonalite	Crd-Grd[a]	Qtz-Diorite	Gabbro	Granodiorite			Tonalite
Sample	NM-1	NM-2	NM-3	NM-4	NM-5	NM-6	NM-7	NM-8
(Wt%)								
SiO_2	59.59	65.75	55.72	47.98	67.26	65.17	64.83	63.82
TiO_2	0.73	0.56	0.75	0.91	0.4	0.67	0.74	0.59
Al_2O_3	15.78	16.05	17.76	19.82	15.58	15.16	15.69	15.7
Fe_2O_3	2.01	1.86	4.04	3.83	2.23	2.95	3.41	2,21
FeO	6.52	3.86	7.48	9.37	3,87	4.95	3.84	5.28
MgO	3.46	2.42	4.32	6.2	1.27	2.06	1.78	2.63
MnO	0.14	0.06	0.16	0.2	0.08	0.11	0.08	0.13
CaO	6.43	4.43	8.26	10.37	4.03	4.62	4.98	5.74
Na_2O	2.74	3.92	2.69	2.16	3.47	3.39	2.96	3.27
K_2O	1.44	1.54	0.71	0.18	2.59	2.35	3.36	1.48
P_2O_5	0.12	0.17	0.1	0.12	0.15	0.13	0.21	0.16
LOI	2.23	0.73	1.11	1.55	0.75	0.75	0.99	0.53
Total	99.18	99.49	99.06	98.86	99.45	99.36	99.46	99.33
(ppm)								
Rb	58	48	30	5	107	88	153	51
Sr	188	379	192	237	174	160	251	274
Y	28	17	23	19	29	32	29	21
Zr	119	136	60	–	198	173	260	138
Nb	6	8	5	6	10	6	9	7
Ba	168	–	2	46	275	–	–	172
La	1.37	2.77	1.48	1.04	0.28	1.64	3.07	0.56
Ce	7.2	11	2.84	2.22	8.57	1.94	14.3	10.5
Sm	1.48	0.83	1	0.68	0.98	0.12	1.23	1.29
Lu	0.35	0.22	0.43	0.32	0.3	0.12	0.17	0.57

[a] Grd: Granodiorite.

higher alumina and alkalis, and lower CaO and MgO contents for the same SiO_2 ranges.

Fig. 6 shows a pseudoternary system defined by Opx-An-Or (Díaz-Alvarado et al., 2011; Castro, 2013). This projection is particularly significant for visualizing magmatic processes in natural rocks and experimental data, according to which different fields have been defined by T, P and H_2O conditions for the generation and the evolution of granitic melts (Castro, 2013 and references therein). Flamenco pluton granitoids trace a cotectic-like evolution from gabbros and Qtz-diorites to tonalites and granodiorites. This trend matches the field described for undersaturated and low-pressure melts, and, as shown in the previous diagrams, are consistent with comparative cordilleran granitoids. Fractionation or cotectic trends are crossed by transverse lines defined by some granitoids from the Flamenco pluton and comparative samples. These are evident in samples from the Copiapó Plutonic Complex and the Limarí-Papudo-Illapel batholith, and in slight deflection, in some granodiorites from the Flamenco samples. Granodiorites (NM-2 and NM-6) outline transverse trends pointing to the compositional fields of graywackes and pelites, in which the metasedimentary rocks of the Las Tórtolas formation (Figs. 6 and 7a) are represented. Anyway, Flamenco samples from Qtz-diorites to granodiorites show a general linear trend and close geochemical characteristics with calc-alkaline cordilleran magmatism (Fig. 7b and c).

Rb and other trace elements associated with K_2O are enriched in more differentiated samples without entailing a variation of the alumina saturation index (ASI) (Table 1, Fig. 7d), which remains constant in all samples, with slight variations in some granodiorites (NM-2, Crd-Granodiorites). The variance between LREE and HREE is represented by the relationship between Lu* and the La*/Lu* ratio (Fig. 7e). The La values are almost identical for all the studied samples. However, the Lu values are lower and, therefore, the LREE/HREE are greater for granodiorites compared to less evolved granitoids. Spider diagrams (Fig. 8a, b) are employed using Thompson MORB normalization and are consistent with average values given by Kelemen et al. (2003) for typical continental arc andesites. The Flamenco pluton samples show typical depletion of Nb and Ti, more outstanding in granodiorites (Fig. 8b), and enrichment in Ba, Rb and K that characterize arc setting magmatism.

5. Thermobarometry and thermal modeling

5.1. Thermobarometry

With the aim of estimating temperatures and pressures reached at the emplacement level of the Flamenco pluton and to assess P-T conditions during granoblastic recrystallization described in some intrusive granitoid facies (see Chapter 3), mineral compositions obtained by electron microprobe analyses were used. Two Qtz-dioritic samples (NM-3 and NA-2) were selected for the thermobarometric study (Fig. 9a). According to mineral assemblages found in granitoids comprising the Flamenco pluton, temperatures have been obtained using Hbl–Pl equilibrium after multiple iterations as a function of the pressure. These temperatures are interpreted as cooling temperatures and can be established as a minimum magma temperature during the emplacement process. Furthermore, when the petrographic study indicated that some granodioritic facies have metamorphic textures (NM-6), Hbl–Pl thermobarometry was used to approach the conditions for the granulitization process. All thermometry results are referred to HB2 temperatures calibrated according to the reaction of edenite + albite = richterite + anorthite (Holland and Blundy, 1994). As a first approach, 2 and 4 Kbars have been selected. The presence of Crd and absence of Grt in the metasedimentary pelitic host rocks settle an upper limit of 4–6 Kbars for pressure conditions (Le Breton and Thompson, 1988; Vielzeuf and Holloway, 1988). Calibrations of the Al-in-hornblende barometer (Schmidt, 1992) have also been used, yielding consistent results with randomly selected pressures. Electron microprobe analyses were conducted with a JEOL JXA-8200 SuperProbe at the University of Huelva. A combination of silicates and oxides were used for calibration. The results are shown in Table 2. The compositions of the analyzed Hbl–Pl pairs are shown in Appendix 1.

Fig. 9 shows BSE images of selected samples for the

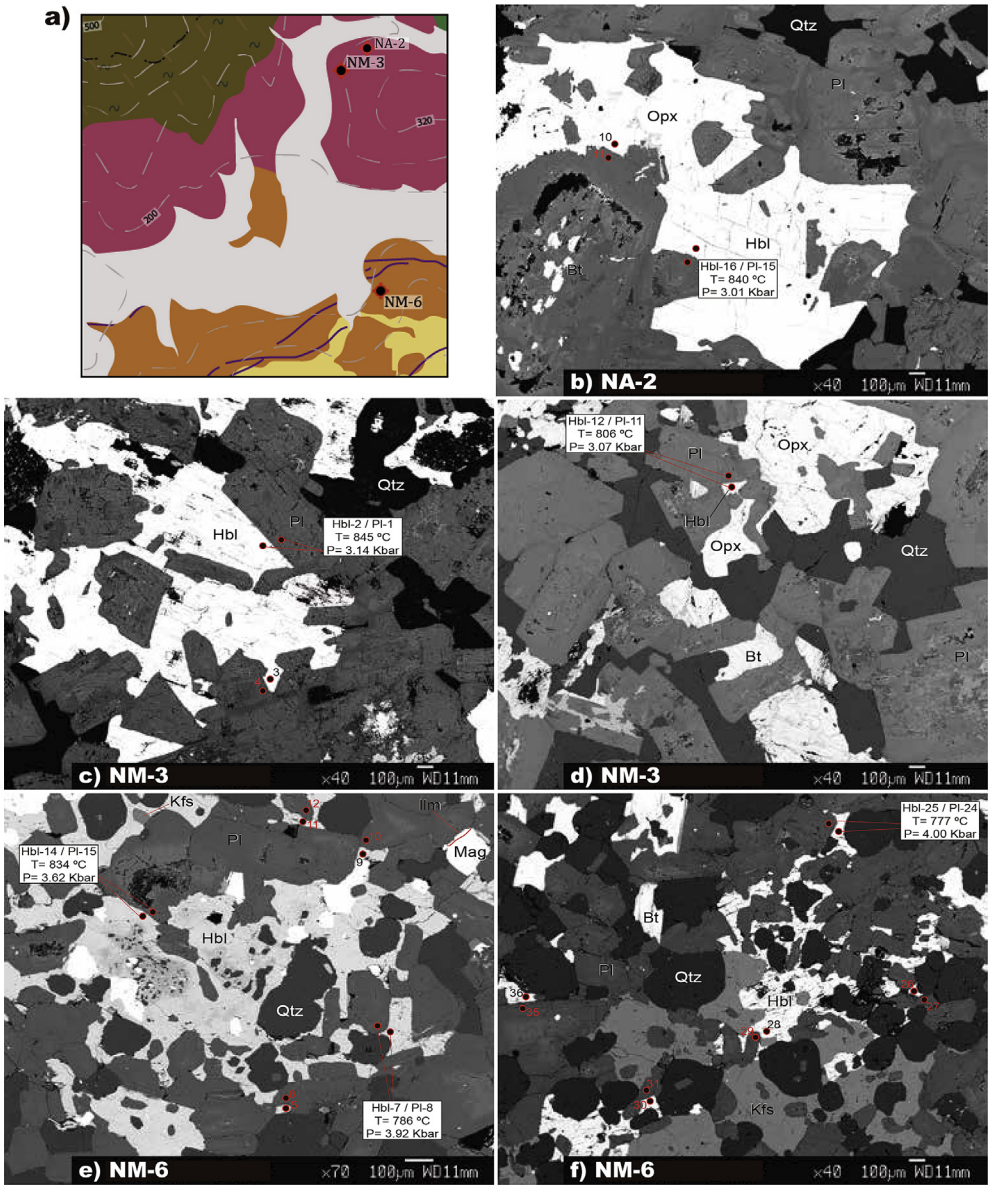

Fig. 9. (a) Detailed geological sketch of the Flamenco north contact with the location of samples selected for the thermobarometric study. (b, c, d) BSE images of NA-2 and NM-3 Qtz-dioritic samples. (e, f) BSE images of the NA-6 granodioritic sample. Microprobe analysis points (Table 2) are indicated with representative results of the Hbl–Pl thermobarometry.

thermobarometric study. Hbl–Pl pairs in the Qtz-diorite samples (Fig. 9b, c) yield constant temperatures from 820 to 850 °C for random and calculated pressures, resulting in Schmidt pressures of 3 ± 0.15 kbars (Table 2). These results are obtained in equilibrium igneous textures. However, the NM-3 sample shows areas where engulfed Opx, interstitial Hbl and triple junctions between Pl and Hbl (Fig. 9d) are observed. Hbl–Pl temperatures are slightly lower in these areas, between 800 and 820 °C.

Leucocratic granodiorites sampled near the Flamenco pluton contact (Fig. 9a) show an almost complete demise of igneous textures because of granoblastic recrystallization observed in these intrusive facies. Qtz-Pl-Hbl triple junctions and interstitial and poikiloblastic Kfs crystallization are dominant over the igneous textures (Fig. 9e, f). Temperatures reached during granulitization are obtained from the Hbl–Pl pairs showing granoblastic textures as a criterion of chemical equilibrium. In areas where the original straight igneous contacts are preserved (Fig. 9e), temperatures approximately 830 °C are maintained. However, where recrystallization processes are evident, temperatures yielded by granoblastic Hbl–Pl pairs are considerably lower (Fig. 9e, f), between 770 and 790 °C (Table 2). Calculated Schmidt pressures are higher than those obtained for NM-3 Qtz-diorites, ca. 4 ± 0.5 kbars Kbars.

The granodioritic intrusive facies with igneous textures show oscillatory zoned Pl. Thermobarometric data calculated between Pl Ca-rich cores (75% An) and zonation absent Hbl, assuming that these phases were previously in equilibrium, give temperatures approximately 900 °C (Table 2). These results should be considered a minimum of the magma temperatures during the emplacement process, whereas temperatures obtained using Pl external rims (50% An) are lower cooling temperatures.

5.2. Thermal modeling

5.2.1. Rationale and model setup

Numerical modeling has been applied to study a wide range of

Table 2
Plagioclase–Hornblende thermobarometry results.

Sample	Hbl	Pl	2 Kbar	4 Kbar	Schmidt		A&S
			T (°C)	T (°C)	T (°C)	P (Kbar)	T (°C)
NA-2	NA2-16	NA2-15	837	844	840	3.01	830
	NA2-10	NA2-11	831	840	835	2.84	824
	NA2-2	NA2-7	821	828	824	2.86	816
	NA2-4	NA2-3	835	843	839	3.00	829
NM-3	NM3-2	NM3-1	842	848	845	3.14	836
	NM3-3	NM3-4	814	823	820	3.32	810
	NM3-12	NM3-11	802	809	806	3.07	799
NM-6	NM6-5	NM6-6	795	801	801	4.18	796
	NM6-7	NM6-8	780	787	786	3.92	781
	NM6-9	NM6-10	795	799	798	3.61	794
	NM6-11	NM6-12	790	796	796	3.80	790
	NM6-14	NM6-15	829	835	834	3.62	826
	NM6-25	NM6-24	770	777	777	4.00	772
	NM6-26	NM6-27	785	792	794	4.57	787
	NM6-28	NM6-29	792	798	799	4.06	792
	NM6-30	NM6-31	771	778	778	4.18	773
	NM6-36	NM6-35	794	798	796	3.18	792
	NM6-5[a]	NM6-3[a]	897	904	904	4.18	889

T (°C): HB2 temperature in Holland and Blundy (1994).
2 and 4 Kbar: results based on an arbitrary pressure.
Schmidt: pressure-based results according to Schmidt's (1992).
A&S: pressure-based results according to Anderson and Smith's (1995).
[a] This Hbl–Pl pair is not in contact. Pl core and unzoned Hbl thermobarometry.

geological processes, as the relation of the magma with the host rock, the residence times of silicic magma chambers, the cooling, emplacement, crystallization and compositional variations of different magma chambers (Annen, 2009; Bachmann and Bergantz, 2004; Bea, 2010; Dufek and Bergantz, 2005; Gelman et al., 2014, 2013; Gutiérrez and Parada, 2010; Koyaguchi and Kaneko, 2000; Molina et al., 2015). Here, the thermal modeling of cooling magma chambers is used to know the thermal effect on the host rock at different conditions of emplacement.

We have simulated 4 case studies of crystallizing magma chambers at different depths, corresponding to 3 and 4 kbar, diverse temperatures of emplacement (Table 3), and redox conditions of one log unite above the QFM oxygen buffer, by the 2D numerical approach solving conductive cooling by finite difference (Wohletz et al., 1999). The FD mesh consists of elements of 100-m-size for both magma and host rock. Modeling of phase equilibria is conducted with the Rhyolite-MELTS code (Gualda et al., 2012), in order to know *liquidus* and crystal fraction evolution regarding the different conditions of emplacement. The composition used for thermal modeling is the tonalite NM-8 because of their abundance along the batholith and the proximity to the parental magma according to field observations.

The purpose of this thermal modeling is to establish the extent and shape of the thermal metamorphic aureole caused by magma intrusion. With this aim, we consider two extreme scenarios for the magma emplacement. In one case, the magma is emplaced with a crystal fraction of 0.5 (case studies 1 and 2: Fig. 10a, b). We use this crystal fraction as upper limit above which the rheological properties would inhibit the magma emplacement (Bachmann and Bergantz, 2004). At the opposite end, the magma intrudes as totally liquid, and temperature of emplacement will be the corresponding to the *liquidus* (case studies 3 and 4: Fig. 10c, d). The thermal modeling covers the entire temperature range from the instantaneous emplacement to the solidification of the whole magma. Temperature of emplacement, magma density and specific heat capacity have been set by Rhyolite-MELTS code according the two scenarios proposed here (Table 3). We range the pressure of emplacement from 4 to 3 kbar, according to the thermobarometry data described in the previous section.

The selected geometry for all case studies is tabular with 20 km of width and 2 km of height, corresponding to a constant volume of 62.83 km^3 (Table 3). Thermal properties for the different case studies are given in Table 3. The thermal gradient imposed for the crust is 30 °C/km (de Silva and Gregg, 2014; Gelman et al., 2013; Huber et al., 2009).

Heat transfer is calculated solved to the conservation of energy:

$$\frac{\partial T}{\partial t} = \nabla \cdot K \nabla T - \boldsymbol{u} \cdot \nabla T + Q \quad (1)$$

where T is magma temperature, t is time, κ is thermal diffusivity, u is the velocity vector, and Q contains heat sources and sinks. The latent heat of crystallization is included in calculations with a constant value of 350 kJ/kg for silicate phases is assumed (Wohletz et al., 1999):

$$\frac{\partial T}{\partial t} = \frac{Q}{(C_p + 1) \cdot T_{SL}} \quad (2)$$

where the latent heat is Q, C_p is the heat capacity and ΔT_{SL} is the temperature interval between *liquidus* and *solidus*.

Thermal conductivity of magma is set at 1.3 and 1.5 W/m °C as initial value depending on the temperature of emplacement (Table 3), and it is considered as dependent on the pressure and temperature according to the equation from (Chapman and Furlong, 1992):

$$K\,(T,z) = K_0 \frac{(1 + cz)}{(1 + bT)} \quad (3)$$

where K(T,z) represents the thermal conductivity variation regarding the temperature (t) and depth (z), K_0 is conductivity at 0 °C, *c* is the crustal depth constant, and *b* is the thermal constant for the upper crust.

Crustal density is fixed at 2800 kg/m^3. Magmatic density and specific heat are estimated by Rhyolite-MELTS code according to the magmatic conditions of emplacement (Table 3). The heat capacity (C_p) for crust is also assumed as constant (1390 J/kg °C; Gutiérrez and Parada, 2010). To simplify the modeling, magma is instantaneously emplaced in a single shoot and further replenishment is not considered (Bea, 2010; Gutierrez and Parada, 2010; Rodriguez et al., 2015). Time step for calculations varies from 15 to 24 years and the grid size used is set at 100 m. The initial temperature distribution of the crust is delimited for the imposed geothermal gradient. Lateral walls of the country rock are considered as insulators.

6. Results

We have performed numerical simulations of cooling magma chambers emplaced at different pressures and temperatures according to the assumptions previously described. We used horizontal thermal profiles at 11 and 14.4 km of depth, depending on the pressure of emplacement, to delimit the distance over which the

Table 3
Case studies designed for the thermal modeling.

Case study	1	2	3	4
Temperature of emplacement (°C)[a]	992	1007	1141.6	1159
Depth of emplacement (km)	11	14.4	11	14.4
Thermal conductivity (W/m°C)	1.5	1.5	1.3	1.3
Specific heat capacity (J/kgK)[a]	1259	1271	1249	1249
Crystal fraction	0.5	0.5	0	0
Volume (km^3)	62.83	62.83	62.83	62.83
Density (kg/m^3)[a]	2641	2655	2524	2541

[a] Parameters estimated by Rhyolite-MELTS.

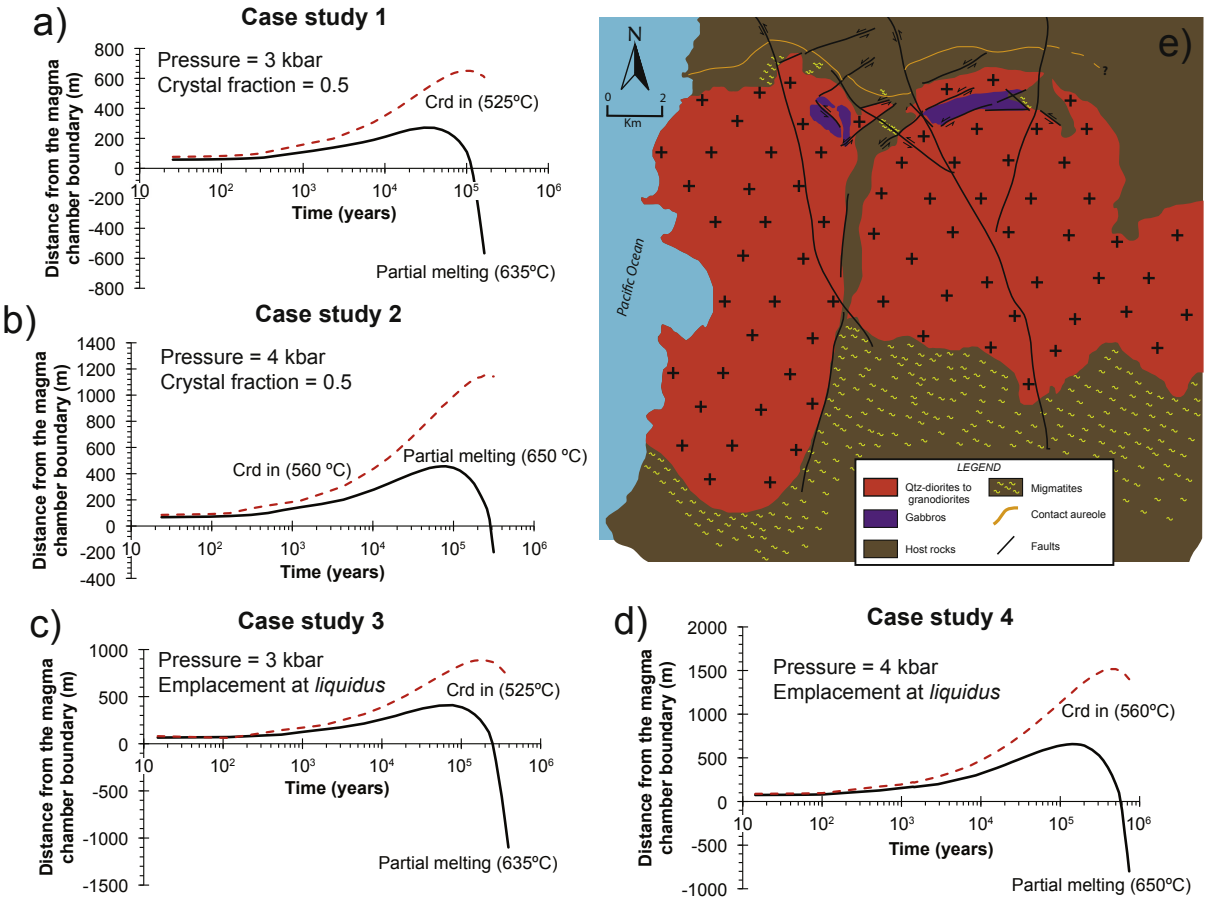

Fig. 10. (a–d) Thermal modeling results for different case studies. The position of both partial melting and Crd-in isograds are represented according to the time elapsed from the magma chamber emplacement for all case studies. Result for magma chambers emplaced at temperatures equivalent to 0.5 of crystal fraction are given in a (T = 992 °C) and b (T = 1007 °C). The isograds resulting from the emplacement at liquidus temperature are showed in c (T = 1141.6 °C) and d (T = 1159 °C) (Table 3). (e) Geological sketch summarizing the main characteristics of the thermal aureole observed in Flamenco pluton. North aureole has been mapped according to the field observations carried out in this study, whereas the south aureole was drawn following the metamorphic aureole described by Grocott and Taylor, 2002.

host is above the temperature of partial melting and cordiertite stabilization. The beginning of the crustal partial melting is estimated to start above 635 °C for 3 kbar of pressure and 650 °C for 4 kbar of pressure (Spear, 1994). These temperatures will be taken as reference to study the zone affected by partial melting in thermal profiles from numerical modeling. The Crd stabilization starts at 525 °C and 560 °C under pressures of 3 and 4 kbar, respectively (Spear, 1994). The position with respect of magma chamber boundary of both isograds is represented with respect to the time for each case study (Fig. 10a to d). The more extended zone affected by partial melting (≈650 m) is found for a totally liquid magma chamber emplaced at 4 kbar (Fig. 10d). In the cases of partially crystallized (X_c = 0.5) and crystal-absent magma chambers emplaced at 3 kbar (Fig. 10a and c, respectively), migmatites are constrained to the first 300–400 m from the pluton boundary. The stabilization of Crd according to the reaction Mg-Chl + Als = Mg-Crd (Spear, 1994) is chiefly influenced by the thermal maturity of the host rock, which is related to imposed pressure conditions. For both emplacement temperatures, Crd-aureoles extend above 1200 m in the cases of magma chambers emplaced at 4 kbar (Fig. 10b, d), whereas they are around 700–800 m in 3 kbar models (Fig. 10a, c).

The simulation of the instantaneous emplacement of a single magmatic pulse that has the dimensions observed in the Flamenco pluton promotes the formation of a homogeneous aureole around the magma chamber. The expected aureole by the magma intrusion expected for the Flamenco pluton emplacement varies their length scale from 650 m (case study 1) to 1500 m (case study 4) (Fig. 10).

7. Discussion

7.1. Geochemical constraints

This study has focused on describing the geochemistry of the granitoids that comprise the Flamenco pluton and the interaction between intrusive magmas and the metasedimentary host rocks at the emplacement level. The extent of the observed interaction and the scarcity of voluminous high-grade metamorphic domains in the Paleozoic basement of the Coastal Range batholith allow us to assess the magma emplacement mechanisms that formed the Flamenco pluton in the Jurassic-Cretaceous magmatic arc in the western margin of South America.

In its northern area, the Flamenco pluton granitoids belong to a calcic, magnesian and metaluminous series, with wide geochemical variability, from gabbros to granodiorites, typical of syn-collisional volcanic arc settings (Fig. 4). Sample plots show a linear evolution trend, characteristic of magmatic fractionation processes (Figs. 5 and 7). These diagrams show a clear compositional affinity between Flamenco samples and calc-alkaline cordilleran batholiths. These patterns are referred to as cotectic lines of liquids (CLL; Castro, 2013), representing liquids fractionating from an

equilibrium saturating solid assemblage at different temperatures. These mineral assemblages are dominated by Px in the less evolved magmas, with a distribution coefficient (D) < 1 for all REEs, and Hbl in granodiorites, in which D is > 1 for the HREE, producing steeper REE patterns (Fig. 7e), and possibly accompanied by Pl, which is characteristic of calc-alkaline systems. Qtz-diorites and tonalites coincide with primary andesitic magma fields and are genetically related to typical compositions of evolved andesites (Green, 1982; Kelemen et al., 2003) (Fig. 8), whereas granodiorites evolve along cotectic experimental lines drawn by liquids developed at undersaturated and low-pressure conditions (Fig. 6). The preponderance of sharp contacts and the absence of gradual transition between granitoid bodies suggest that differentiation processes from Qtz-diorites to granodiorites do not occur in-situ at the emplacement level. Cotectic trends plotted from the Flamenco samples are consistent with the compositional fields of huge paradigmatic cordilleran batholiths (Peninsular Range: Lee et al., 2007; Patagonia: Hervé et al., 2007; Pankhrust et al., 1999); and available geochemical data indicates that other Coastal Cordillera batholiths are spatially and temporally related to the Flamenco pluton (Copiapó Plutonic Complex: Marschik et al., 2003; and Limarí-Papudo-Illapel batholith: Parada et al., 1999) (Figs. 5–7).

Some field relations and variations in the geochemical trends described here are representative of the interaction between the intrusive magma and the metasedimentary host rocks. According to petrographic descriptions, the presence in some granodiritic facies (NM-2) of large prismatic euhedral pinnite-biotite crystals, typical of Crd pseudomorphs (Fig. 2f), as well as polycrystalline Qtz xenocrysts are related to assimilation processes. The peritectic euhedral Crd crystallizes in magmatic environments where xenolithic pelite melting reactions occur (Erdmann et al., 2007; Diaz-Alvarado et al., 2011). Furthermore, some granodioritic samples are enriched in MgO and alkalis, coupled with an increasing alumina saturation index (Figs. 4c and 5). These are traces of local contamination with pelitic country rocks (Díaz-Alvarado et al., 2011; Castro et al., 2014; Bellos et al., 2015). FM-An-Or (Fig. 6) and CaO vs MgO (Fig. 7a) are definite projections to expose and measure the extension of assimilation processes (Díaz-Alvarado et al., 2011). NM-2 and NM-6 granodiorites show crossed trends related to fractionation linear arrangements, pointing to pelites and graywackes in the field. Therefore, assimilation processes that involve Flamenco granitoids produce small scale geochemical variations, and further limited to those areas near the contacts. Interaction processes are mostly mechanical, and a short range geochemical assimilation is limited to a few meters along the contact.

7.2. Deformational phases and emplacement

There is a significant relationship between deformational phases and structures, the space generation, and the emplacement and formation of large batholiths. Thus, the Jurassic-Cretaceous magmatic arc in the Coastal Cordillera in northern Chile provides an exceptional example of magmatism relating the tectonic inversion deformation at a convergent margin that has evolved from extensional tectonics, framed in a retreating subduction boundary context in the Early Jurassic to Early Cretaceous, to compressive tectonics (Williams et al., 1989; Arévalo and Grocott, 1997; Grocott and Taylor, 2002).

At the northern contact, the Flamenco pluton is emplaced in a phyllite-quartzite succession with volcano-sedimentary rocks of the Las Tórtolas formation. The study area has been divided into three zones according to their structural characteristics (Fig. 1d). To the west, melange facies show a total dismantling of the original turbidite architecture, presenting a planar-linear fabric and a NW–SE trending main stretching lineation. This deformation has been dated as Late Carboniferous (Bell, 1987). Similar orientations are observed in the stretching lineations marked by granoblastic Crd in the contact aureole (Fig. 2d), but framed by contact metamorphism during the Early Jurassic intrusive process. This extensional deformation phase could be syn-tectonic with boudinage structures described in the volcanic rocks of the study area (Fig. 2b), and coincides with crustal-scale N–S to NWN-SES trending detachments, with top to east kinematics that determine the main emplacement episode (D2 phase, Grocott and Taylor, 2002). Additionally, this is consistent with the main NW–SE orientation of the tabular intrusive sheets that form the Flamenco pluton (Grocott and Wilson, 1997). Grocott and Taylor (2002) described the subsequent D3 and D4 phases as a result of the roof uplift and pluton filling with high emplacement rates related to space generation. The presence of straight or slightly inclined folds and steeped foliations and lineations measured throughout the study area correlate with these deformational phases. Syn-emplacement structures fold the Crd-schists that belong to the contact aureole generated during the early intrusive phases.

Thrust faults and associated propagation folds in the east of the study area that promote the auto-thrusting of boudin blocks crosscut the previous structures. There is no precise dating of these structures, and they may develop during horizontal flattening proposed for the late emplacement process (Grocott and Taylor, 2002) or during the crustal scale tectonic compressive phase at the continental margin.

7.3. Self-granulitization and thermal aureole

According to the assemblage of various geochemically distinguishable granitic facies and to the variety of structures generated during pluton building, the Flamenco pluton was formed during a protracted emplacement process. Qtz-dioritic and granodioritic magmatic facies (NM-3 and NM-6 samples) described in the northern margin of the pluton show granulitization textures and temperatures, acquired during the successive intrusion of magmatic pulses. Temperatures of 780 ± 10 °C recorded by granoblastic Hbl–Pl equilibriums (Fig. 9) represent the response of previously emplaced granitoids to the thermal input of subsequent intrusive stages. In this sense, self-granulitization and the observed sharp contacts between the different magmatic facies suggest that the first pulses are close to or below its *solidus* temperature during sucessive intrusive phases. This may also be caused by the thermal immaturity of the crust in the early stages of the pluton building.

The hypothesis of the sequential emplacement for the formation of Flamenco pluton, and the scarcity of extensive high-grade domains in the fertile metasedimentary host rocks of the Coastal Range batholith, have been contrasted with the 2D thermo-numerical model of a magma chamber with similar dimensions to the Flamenco pluton (Fig. 10). Therefore, it has been possible to compare the development of the observed thermal aureole and that calculated by the thermal modeling. Firstly, the thermal aureole predicted by the 2D model show a homogeneous shape and development around the pluton, whereas the observed aureole presents further development to the south, and a very irregular shape in the north area of the Flamenco pluton (Fig. 10e). The proposed emplacement temperatures for the case studies are between 992 and 1159 °C for intrusive magmas (Table 3), far above the minimum temperature yield by the Hbl–Pl thermobarometry (900 °C, Table 2). The model results also show the influence of the depth of emplacement for the development of the contact aureole (Table 3, Fig. 10).

According to the proposed model, the established temperatures for the melting reactions in the host-rocks can be located at distances between 200 and 650 m from the magma chamber

boundary (Fig. 10), depending on the fixed initial conditions and for elapsed times of 10^5 years from the magma emplacement. The high-grade conditions are achieved and maintained for longer times in the case study of emplacement at liquidus temperatures and 4 kbar. However, the south contact of the Flamenco pluton presents a noteworthy domain of migmatitic rocks (distances from the pluton contact up to 2 Km, Grocott and Taylor, 2002), as in the north contact, in spite of presenting tectonic contacs, migmatite outcrops are scarce and Crd-schists are limited to, at most, the first kilometer from the contact (Fig. 10e). Thus, the irregular development of the contact aureole observed in the Flamenco pluton, in comparison with that obtained by thermo-numerical modeling, together with the self-granulitization processes described in marginal magmatic facies in the north area, point to a sequential building for the pluton. To explain this irregularity of the contact aureole and the presence of large migmatitic domains in the south, it is necessary to invoke an intrusive complex growth by accretion from north to south (in its current location), allowing the high-grade aureole development of the host rocks in this area.

8. Concluding remarks

The descriptions of granitoids with granulitic textures in the pluton margins and the contact metamorphism aureoles point to the conditions in which the Flamenco pluton has been built. Thus, in the framework of the theoretical limits established by the simple 2D thermal modeling approach, we find first-order constraints on the thermal response of the host crust, and setting the emplacement mechanisms of intrusive magmas. Therefore, the processes of self-granulitization and the irregular contact aureole described in this paper indicate that the Flamenco pluton is formed by a protrated process of repeated intrusion of magma pulses, as is pointed by the presence of folded aureole rocks. The successive emplacement is preferably located over previous granitoid batches. Otherwise, the accumulation of intrusive pulses in the crust would generate a higher thermal maturity in the host-rocks, although this also has been shown to be related to emplacement rates, and would increase the interaction processes between granitic melts and metasediments.

Acknowledgments

This work has been developed during the PhD Thesis proposal of Natalia Rodríguez, carried out at the Department of Geology of the University of Atacama. The work was funded with FONDECYT Project Nº 11140722 of CONICYT, and with the fund support of DIUDA 2013-22268 and DIUDA 2014-22273 projects. We are grateful for constructive colleague reviews by Gustavo Miranda and Wolfgang Griem, all of which improved the manuscript.

We would like to sincerely thank the Editor-in-Chief, the Regional Editor (Reinaldo Charrier) and the reviewers of Journal of South American Earth Sciences for their thorough corrections of the first draft of this manuscript.

Appendix 1

Table A1
Electron microprobe analysis of Hbl–Pl pairs used in thermobarometry.

Sample	NA-2								NM-3						NM-6			
Hbl–Pl pairs	Hbl-16	Pl-15	Hbl-10	Pl-11	Hbl-2	Pl-7	Hbl-4	Pl-3	Hbl-2	Pl-1	Hbl-3	Pl-4	Hbl-12	Pl-11	Hbl-5	Pl-6	Hbl-7	Pl-8
SiO_2	47.41	54.26	47.87	53.93	47.48	55,27	47.20	53.47	46.70	53.93	47.21	53.56	46.85	56.50	43.73	59.57	44.95	59.95
TiO_2	1.21	0.00	1.29	0.04	1.34	–	1.15	0.02	1.22	–	0.99	–	0.65	0.05	1.23	0.04	1.38	0.04
Al_2O_3	7.31	29.35	7.11	29.46	7.11	28.58	7.27	29.14	7.43	28.91	7.68	29.55	7.32	28.08	8.40	26.03	8,22	25.77
FeO	16.41	0.20	15.19	0.18	16.00	0.16	16.59	0.22	16.12	0.09	16.66	0.15	17.93	0.18	20.51	0.25	19.72	0.27
MgO	12.58	0.00	13.05	–	12.63	0.02	12.53	0.04	12.84	–	12.37	–	12.45	0.03	8.68	–	9.27	–
MnO	0,40	–	0.33	0.02	0.35	–	0.45	0.01	0.38	–	0.37	0.02	0.55	0.01	0.76	–	0.79	0.03
CaO	10.83	11.32	11.05	11.61	11.08	10.50	10.70	11.26	10.73	10.66	10.87	11.42	9.85	9.60	11.43	7.25	11.46	6.96
Na_2O	0.87	5.00	0.90	4.92	0.88	5.52	0.84	5.14	0.88	5.56	0.78	5.01	0.78	6.10	1.05	7.24	1.12	7.37
K_2O	0.39	0.06	0.35	0.06	0.37	0.11	0.37	0.10	0.35	0.03	0.39	0.08	0.35	0.09	0.97	0.17	0.92	0.17
P_2O_5	0.00	–	–	0.04	0.01	0.01	0.01	0.01	0.01	0.01	–	0.03	–	0.01	0.01	–	–	0.02
NiO	0.02	–	0.09	–	0.03	–	0.06	0.07	–	–	–	–	–	–	–	0.00	0.05	–
Cr_2O_3	0.09	–	–	–	–	0.04	–	0.04	0.07	0.05	–	0.08	0.04	0.04	0.03	–	0.09	0.01
SrO	–	0.01	–	0.02	0.01	–	–	–	0.01	–	0.02	0.02	–	0.03	–	0.06	–	0.01
BaO	0.04	–	0.07	0.07	0.01	0.01	–	–	–	–	–	0.02	–	0.03	0.01	–	0.03	0.04
SO_3	–	–	0.02	–	–	0.02	0.00	0.03	–	–	–	0.01	0.00	–	–	0.03	0.01	0.01
F	0.03	–	0.21	0.02	–	0.19	0.01	0.13	0.02	–	–	–	–	–	0.14	–	–	–
Total	97.59	100.20	97.44	100.36	97.29	100.34	97.18	99.63	96.75	99.25	97.33	99.94	96.75	100.73	96.89	100.62	97.98	100.63
Sample	NM-6																	
Hbl–Pl pairs	Hbl-9	Pl-10	Hbl-11	Pl-12	Hbl-14	Pl-15	Hbl-25	Pl-24	Hbl-26	Pl-27	Hbl-28	Pl-29	Hbl-30	Pl-31	Hbl-36	Pl-35	Hbl-5	Pl-3
SiO_2	45.08	60.17	45.08	59.59	45.06	58.18	44.85	59.89	44.05	59.65	44.71	58.59	44.60	59.63	45.16	60.25	43.73	53.13
TiO_2	1.30	0.04	1.31	–	1.61	0.00	1.43	–	1.32	0.00	1.26	0.04	1.39	0.06	1.24	0.02	1.23	0.05
Al_2O_3	7.88	25.43	8.09	25.60	7.85	26.49	8.31	25.49	8.98	25.68	8.38	26.14	8.51	25.55	7.29	25.17	8.40	30.22
FeO	20.03	0.26	20.12	0.25	19.45	0.23	20.07	0.22	20.56	0.21	20.02	0.11	19.87	0.09	19.27	0.23	20.51	0.18
MgO	9.58	0.01	9.29	–	9.50	0.01	9.09	0.01	8.80	–	9.22	0.01	9.12	0.00	9.90	–	8.68	0.00
MnO	0.79	0.00	0.70	–	0.75	0.02	0.69	–	0.70	0.02	0.73	0.02	0.67	–	0.66	–	0.76	–
CaO	11.43	6.59	11.34	6.77	11.13	7.95	11.42	6.49	11.57	6.96	11.40	7.39	11.50	6.70	11.19	6.48	11.43	12.35
Na_2O	1.01	7.77	1.22	7.40	1.31	6.92	1.15	7.87	1.17	7.58	1.09	7.33	1.18	7.69	1.16	7.73	1.05	4.55
K_2O	0.87	0.18	0.90	0.19	0.92	0.15	0.93	0.15	0.98	0.21	0.93	0.15	0.97	0.20	0.79	0.23	0.97	0.12
P_2O_5	–	0.00	–	0.01	0.04	0.00	0.01	–	–	0.02	–	0.00	–	–	–	0.04	0.01	–
NiO	0.03	0.03	0.03	–	0.03	0.01	0.01	–	0.02	–	–	–	–	0.02	–	0.01	–	0.03
Cr_2O_3	–	0.01	–	–	–	0.02	–	0.05	0.02	0.02	0.04	–	–	–	–	0.04	0.03	0.04
SrO	–	0.02	–	–	0.01	0.04	–	–	–	0.03	–	0.04	0.01	0.00	0.01	0.01	–	0.08
BaO	–	0.04	–	–	–	0.01	0.00	–	0.00	0.08	0.03	0.05	–	0.03	0.08	0.02	0.01	–
SO_3	0.02	–	0.01	–	0.00	0.01	0.02	–	0.02	–	–	0.01	–	0.02	0.03	–	–	0.00
F	0.21	–	–	–	0.10	–	0.21	0.03	0.18	–	0.15	–	0.01	0.07	0.07	0.03	0.14	–
Total	98.14	100.55	98.09	99.80	97.72	100.04	98.10	100.18	98.29	100.46	97.89	99.88	97.83	100.03	96.83	100.25	96.89	100.75

References

Aguirre, L., Herve, F., Godoy, E., 1972. Distribution of metamorphic facies in Chile, an outline. Kristalinikum 9, 7–19.

Anderson, J.L., Smith, D.R., 1995. The effect of temperature and oxygen fugacity on Al-in-hornblende barometry. Am. Mineralogist 80, 549–559.

Annen, C., Sparks, R.S.J., 2002. Effects of repetitive emplacement of basaltic intrusions on thermal evolution and melt generation in the crust. Earth Planet. Sci. Lett. 203, 937–955.

Annen, C., Scaillet, B., Sparks, R.S.J., 2006. Thermal constraints on the emplacement rate of a large intrusive complex: the Manaslu leucogranite, Nepal Himalaya. J. Petrol. 47, 71–95.

Annen, C., 2009. From plutons to magma chambers: Thermal constraints on the accumulation of eruptible silicic magma in the upper crust. Earth Planet. Sci. Lett. 284 (3–4), 409–416.

Annen, C., 2011. Implications of incremental emplacement of magma bodies for magma differentiation, termal aureole dimensions and plutonism-volcanism relationships. Tectonophysics 500, 3–10.

Arévalo, C., Grocott, J., 1997. The tectonic setting of the Chañarcillo group and the Bandurrias formation: an early-late cretaceous sinistral transpressive belt between the coastal cordillera and the precordillera, Atacama region, Chile: Congreso Geológico Chileno. In: 8th, Antofagasta, 1997. Actas 3, pp. 1604–1607.

Bachmann, O., Bergantz, G.W., 2004. On the origin of crysytal-poor rhyolites: extracted from batholitic crystal mushes. J. Petrol. 45, 1565–1582.

Bahlburg, H., Breitkreutz, C., Zeil, W., 1986. Paläozoische Sedimente Nordchiles. Berliner Geowissenschaftliche Abhandlungen, Reihe A 66, 147–168.

Bea, F., 2010. Crystallization dynamics of granite magma chambers in the absence of regional stress: multiphysics modeling with natural examples. J. Petrol. 51, 1541–1569.

Beard, J.S., Ragland, P.C., Crawford, M.L., 2005. Reactive bulk assimilation: a model for the crust-mantle mixing in silicic magmas. Geology 33, 681–684.

Bell, C.M., 1982. The Lower Paleozoic metasedimentary basement of the coastal range of Chile between 25°30' and 27°S. Rev. Geol. Chile 9 (3), 21–29.

Bell, C.M., 1987. The origin of the upper paleozoic chañaral mélange of N Chile. J. Geol. Soc. Lond. 144, 599–610.

Bellos, L.I., Castro, A., Díaz-Alvarado, J., Toselli, A., 2015. Multi-pulse cotectic evolution and in-situ fractionation of calc-alkaline tonalite–granodiorite rocks, Sierra de Velasco batholith, Famatinian belt, Argentina. Gondwana Res. 27, 258–280.

Berg, K., Breitkreuz, C., 1983. Mesozoische Plutone in der nordchilenischen Küstenkordillere: Petrogenese, Geochronologie, Geochemie und Geodynamik mentelbetonter Magmatite. Geotekt. Forschungen 66, 107.

Berg, K., Breitkreuz, C., Damm, K.W., Pichowiak, S., Zeil, W., 1983. The North-Chilean Coast Range - an example for the development of an active continental margin. Geol. Rundsch. 72, 715–731.

Berg, K., Baumann, A., 1985. Plutonic and metasedimentary rocks from the Coastal range of northern Chile. Rb-Sr and U-Pb isotope systematics. Earth Planet. Sci. Lett. 75, 101–115.

Bohrson, W.A., Spera, F.J., 2001. Energy-constrained open system magmatic processes II: application of energy-constrained assimilation-fractional crystallization (EC-AFC) model to magmatic systems. J. Petrol. 42 (5), 1019–1041.

Brook, M., Pankhurst, R., Sheperd, T., Spiro, B., Snelling, N., Swainbank, I., 1986. Andean Geochronology and Metallogenesis. Overseas Development Administration. Open File Report, 83 p, London.

Burgisser, A., Bergantz, C.W., 2011. A rapid mechanism to remobilize and homogenize highly crystalline magma bodies. Nature 471, 212–215.

Castro, A., 2013. Tonalite–granodiorite suites as cotectic systems: a review of experimental studies with application to granitoid petrogenesis. Earth Sci. Rev. 124, 68–95.

Castro, A., Díaz-Alvarado, J., Fernández, C., 2014. Fractionation and incipient self-granulitization during deep-crust emplacement of Lower Ordovician Valle Fértil batholith at the Gondwana active margin of South America. Gondwana Res. 25, 685–706.

Castro, A., 2014. The off-crust origin of granite batholiths. Geosci. Front. 5, 63–75.

Chapman, D.S., Furlong, K.P., 1992. Thermal state of the Continental Lower Crust. Elsevier, Amsterdam.

Charrier, R., Pinto, L., Rodríguez, M.P., 2007. Tectonostratigraphic evolution of the Andean orogen in Chile. In: Moreno, T., Gibbons, W. (Eds.), The Geology of Chile, the Geological Society, Londres, pp. 21–114.

Clemens, J.D., Stevens, G., Farina, F., 2011. The enigmatic sources of I-type granites: the peritectic connexion. Lithos 126 (3–4), 174–181.

Clemens, J.D., Stevens, G., 2012. What controls chemical variation in granitic magmas? Lithos 134–135, 317–329.

Condie, K.C., 1998. Episodic continental growth and supercontinents: a mantle avalanche connection? Earth Planet. Sci. Lett. 163, 97–108.

Condie, K.C., 2000. Episodic continental growth models: afterthoughts and extensions. Tectonophysics 322, 153–162.

Coleman, D.S., Gray, W., Glazner, A.F., 2004. Rethinking the emplacement and evolution of zoned plutons: geochronologic evidence for incremental assembly of the Tuolumne Intrusive Suite, California. Geology 32, 433–436.

Dallmeyer, R.D., Brown, M., Grocott, J., Taylor, G.K., Treloar, P.J., 1996. Mesozoic magmatic and tectonics events within the Andean Plate boundary zone, 26°-27°30'S, North Chile: constraints from 40Ar/39Ar Mineral ages. J. Geol. 104 (1), 19–40.

de Silva, S.L., Gregg, P.M., 2014. Thermomechanical feedbacks in magmatic systems: implications for growth, longevity, and evolution of large caldera-forming magma reservoirs and their supereruptions. J. Volcanol. Geotherm. Res. 282, 77–91.

Díaz, F., 1986. Hoja Salvador, borradores de terreno (Inédito). Servicio Nacional de Geología y Minería, Santiago.

Díaz Alvarado, J., Castro, A., Fernández, C., Moreno-Ventas, I., 2011. Assessing bulk assimilation in cordierite-bearing granitoids from the central system batholith, Spain; experimental, geochemical and geochronological constraints. J. Petrol. 52, 223–256.

Díaz Alvarado, J., Fernández, C., Díaz Azpiroz, M., Castro, A., Moreno-Ventas, I., 2012. Fabric evidence for granodiorite emplacement with extensional shear zones in the Variscan Gredos massif (Spanish Central System). J. Struct. Geol. 42, 74–90.

Díaz-Alvarado, J., Castro, A., Fernández, C., Moreno-Ventas, I., 2013. SHRIMP U–Pb zircon geochronology and thermalmodeling of multilayer granitoid intrusions. Implications for the building and thermal evolution of the central system batholith, Iberian Massif, Spain. Lithos 175–176, 104–123.

Dufek, J., Bergantz, G.W., 2005. Lower crustal magma genesis and preservation: a stochastic framework for the evaluation of basalt–crust interaction. J. Petrol. 46 (11), 2167–2195.

Erdmann, S., London, D., Morgan, G.B., Clarke, D.B., 2007. The contamination of granitic magma by metasedimentary country-rock material: an experimental study. Can. Mineralogist 45, 43–61.

Farrar, E., Clark, A., Haynes, J., Quirt, G., Conn, H., Zentilli, M., 1970. K-Ar evidence for the post-Paleozoic migration of granitic intrusion foci in the Andes of northern Chile. Earth Planet. Sci. Lett. 10, 60–66.

Frost, B.R., Barnes, C.G., Collins, W.J., Arculus, R.J., Ellis, D.J., Frost, C.D., 2001. A geochemical classification for granitic rocks. J. Petrol. 42, 2033–2048.

Gelman, S.E., Gutierrez, F.J., Bachmann, O., 2013. On the longevity of large upper crustal silicic magma chambers. Geology 41, 759–762.

Gelman, S.E., Deering, C.D., Bachmann, O., Huber, C., Gutiérrez, F.J., 2014. Identifying the crystal graveyards remaining after large silicic eruptions. Earth Planet. Sci. Lett. 403, 299–306.

Glazner, A.F., Bartley, J.M., Coleman, D.S., Gray, W., Taylor, R.Z., 2004. Are plutons assembled over millions of years by amalgamation from small magma chambers. GSA Today 14, 4–11.

Godoy, E., 1997. El Gabro Orbicular de Quebrada Animas Viejas, provincia de Chañaral, Chile. In: Congreso Geológico Chileno No. 8, Actas, 2, pp. 1285–1289, (Antofagasta).

Godoy, E., Lara, L., 1998. Hojas Chañaral y Diego de Almagro. Servicio Nacional de Geología y Minería. Mapas Geológicos, 5–6 (1:100.000), Santiago.

González, G., Scheuber, E., 1997. La tectónica del arco magmático del Jurásico-Cretácico Inferior, Cordillera de la Costa (22–26°S), Norte de Chile: Una historia de Deformación cortical en un límite de placas convergentes. In: Proceedings 7th. Congreso Geológico Chileno, Universidad Católica del Norte, Antofagasta (Chile).

Green, T.H., 1982. Anatexis of mafic crust and high pressure crystallization of andesite. In: Thorpe, R.S. (Ed.), Andesites: Orogenic Andesites and Related Rocks. JohnWiley, Chichester, pp. 465–487.

Grocott, J., Brown, M., Dallmeyer, R.D., Taylor, G.K., Treloar, P.J., 1994. Mechanism of continental growth in extensional arcs: an example from de Andean plate-boundary zone. Geology 22, 391–394.

Grocott, J., Wilson, J., 1997. Ascent and emplacement of granitic plutonic complexes in subduction-related extensional environments. Holness, M., Deformation-enhanced Fluid Transport in the Earth's Crust and Mantle. Mineralogical Society Series 7, 173–195.

Grocott, J., Taylor, G.K., 2002. Magmatic arc fault systems, deformation partitioning and emplacement of granitic complexes en the Coastal Cordillera, north Chilean Andes (25°30'S to 27°30'S). J. Geol. Soc. Lond. 159, 425–442.

Gualda, G.A.R., Ghiorso, M.S., Lemons, R.V., Carley, T.L., 2012. Rhyolite-MELTS: a modified calibration of MELTS optimized for silica-rich, fluid-bearing magmatic systems. J. Petrol. 53, 875–890.

Gutiérrez, F., Parada, M.A., 2010. Numerical modeling of time-dependent fluid dynamics and differentiation of a shallow basaltic magma chamber. J. Petrol. 51, 731–762.

Herve, F., Pankhurst, R.J., Fanning, C.M., Calderon, M., Yaxley, G.M., 2007. The South Patagonian batholith: 150 my of granite magmatism on a plate margin. Lithos 97, 373–394.

Holland, T., Blundy, J., 1994. Non-ideal interactions in calcic amphiboles and their bearing on amphibole-plagioclase thermometry. Contrib. Mineral. Pet. 116, 433–447.

Huber, C., Bachmann, O., Manga, M., 2009. Homogenization processes in silicic magma chambers by stirring and mushification (latent heat buffering). Earth Planet. Sci. Lett. 283, 38–47.

Huppert, H.E., Sparks, S.J., 1988. The generation of granitic magma by intrusion of basalt into continental crust. J. Petrol. 29 (3), 599–624.

Kelemen, P.B., Hanghoj, K., Greene, A.R., 2003. One view of the geochemistry of subduction-related magmatic arcs, with emphasis on primitive andesite and lower crust. In: Rudnick, R.L. (Ed.), The Crust. Elsevier, Amsterdam, pp. 593–659.

Kemp, A.I.S., Hawkesworth, 2003. Granitic perspectives on the generation and secular evolution of the continental crust. In: Holland, H.D., Turekian, K.K., Rudnick, R.L. (Eds.), The Crust. Treatise on Geochemistry, vol. 3. Elsevier Pergamon, Oxford, pp. 349–410.

Koyaguchi, T., Kaneko, K., 2000. Thermal evolution of silicic magma chambers after

basalt replenishment. Trans. R. Soc. Edimburgh 91, 47–60.
Kretz, R., 1983. Symbols for rock-forming minerals. Am. Mineralogist 68, 277–279.
Le Breton, N., Thompson, A.B., 1988. Fluid-absent (dehydration) melting of biotite in metapelites in the early stages of crustal anatexis. Contributions Mineralogy Petrol. 99, 226–237.
Lee, C.-T.A., Morton, D.M., Kistler, R.W., Baird, A.K., 2007. Petrology and tectonics of Phanerozoic continent formation: from island arcs to accretion and continental arc magmatism. Earth Planet. Sci. Lett. 263, 370–387.
Levi, B., Aguirre, L., 1981. Ensialic spreading-subsidence in the mesozoic and Paleogene of central Chile. J. Geol. Soc. Lond. 138, 75–81.
Marschik, R., Fontignie, D., Chiaradia, M., Voldet, P., 2003. Geochemical and Sr-Nd-Pb-O isotope composition of granitoides of the Early Cretaceous Copiapó plutonic complex (27°30′S), Chile. J. S. Am. Earth Sci. 16, 381–398.
Menand, T., Daniels, K., Benghiat, P., 2010. Dyke propagation and sill formation in a compressive tectonic environment. J. Geophys. Res. 115, 1–12.
Menand, T., Annen, C., Saint Blanquat, M., 2015. Rates of magma transfer in the crust: Insights into magma reservoir recharge and pluton growth. Geology 43 (3), 199–202.
Michaut, C., Jaupart, C., 2011. Two models for the formation of magma reservoirs by small increments. Tectonophysis 500, 34–49.
Miller, H., 1970. Vergleichende Studien an prämesozoischen Gesteinen Chiles unter besonderer Berücksichtigung ihrer Kleintektonik. Geotekt. Forschungen 36, 64.
Miller, J.S., Matzel, J.E.P., Miller, C.F., Burgess, S.D., Miller, R.B., 2007. Zircon growth and recycling during the assembly of large, composite arc plutons. J. Volcanol. Geotherm. Res. 167, 282–299.
Miller, C.F., Furbish, D.J., Walker, B.A., Claiborne, L.L., Koteas, G.C., Bleick, H.A., Miller, J.S., 2011. Growth of plutons by incremental emplacement of sheets in crystal rich host: evidence from Miocene intrusions of the Colorado River region, Nevada, USA. Tectonophysics 500, 65–77.
Molina, P.G., Parada, M.A., Gutiérrez, F.J., Ma, C., Li, J., Yuanyuan, L., Reich, M., Aravena, Á., 2015. Protracted late magmatic stage of the Caleu pluton (central Chile) as a consequence of heat redistribution by diking: Insights from zircon data and thermal modeling. Lithos 227, 255–268.
Mpodozis, C., Kay, S.M., 1990. Provincias magmáticas acidas y evolución tectónica de Gondwana: Andes Chilenos (28-31°S). Rev. Geol. Chile 17 (2), 153–180.
Mpodozis, C., Ramos, V.A., 2008. Tectónica Jurásica en Argentina y Chile: extensión, subducción oblicua, rifting, deriva y colisiones? Rev. Asoc. Geol. Argent. 63 (4), 481–497.
Naranjo, J.A., Puig, A., 1984. Hojas Taltal y Chañaral, regiones de Antofagasta y Atacama, Servicio Nacional de Geología y Minería, Carta Geológica de Chile, No. 62-63, 140 p., 1 mapa escala 1:250.000, Santiago.
Pankhurst, R.J., Weaver, S.D., Hervé, F., Larrondo, P., 1999. Mesozoic-cenozoic evolution of the North Patagonian batholith in Aysen, southern Chile. J. Geol. Soc. 156, 673–694.
Parada, M.A., Nyström, J.O., Levi, B., 1999. Multiple sources for the Coastal Batholith of central Chile (31-34°S) geochemical and Sr-Nd isotopic evidence and tectonic implications. Lithos 46, 504–521.
Paterson, S.R., Okaya, D., Memeti, V., Economos, R., Miller, R.B., 2011. Magma addition and flux calculations of incrementally constructed magma chambers in continental margin arcs: combined field, geochronologic, and thermal modeling studies. Geosphere 7, 1439–1468.
Pearce, J.A., Harris, N.B.W., Tindle, A.G., 1984. Trace element discrimination diagrams for the tectonic interpretation of granitic rocks. J. Petrol. 25, 956–983.
Plank, T., Langmuir, C.H., 1998. The chemical composition of subducting sediment and its consequences for the crust and mantle. Chem. Geol. 145, 325–394.
Ramos, V.A., 1999. Plate tectonic setting of the Andean cordillera. Episodes 22 (3), 183–190.
Rodríguez, C., Geyer, A., Castro, A., Villaseñor, A., 2015. Natural equivalents of thermal gradient experiments. J. Volcanol. Geotherm. Res. 298, 47–58.
Saint Blanquat, M., Horsman, E., Habert, G., Morgan, S., Vanderhaeghe, O., Law, R., Tikoff, B., 2011. Multiscale magmatic cyclicity, duration of pluton construction, and the paradoxical relationship between tectonism and plutonism in continental arcs. Tectonophysics 500, 20–33.
Saito, S., Arima, M., Nakajima, T., 2007. Hybridization of a shallow 'I-type' granitoid pluton and its host migmatite by magma-chamber wall collapse: TheTokuwa pluton, Central Japan. J. Petrol. 48, 79–111.
Schmidt, M.W., 1992. Amphibole composition in tonalite as a function of pressure: an experimental calibration of the Al-in-hornblende barometer. Contributions Mineralogy Petrol. 110, 304–310.
Spear, F.S., 1994. Metamorphic Phase Equilibria and Pressure-temperature-time Paths. Mineralogical Society of America Monograph, p. 799.
Ulriksen, C., 1979. Regional Geology, Geochronology and Metallogeny of the Coastal Cordillera of Chile between 25° 30' y 26°00'S. Dalhousie University, Halifax, Canada, p. 221. M.Sc. Thesis (Unpublished).
Vielzeuf, D., Holloway, J.R., 1988. Experimental determination of the fluid-absent melting relations in the pelitic system. Contributions Mineralogy Petrol. 98, 257–276.
Vilas, J.F., Valencio, D.A., 1978. Paleomagnetism of south American and African rocks and the age of the south Atlantic. Rev. Bras. Geociências 8, 3–10.
Vogt, K., Gerya, T.V., Castro, A., 2012. Crustal growth at active continental margins: numerical modeling. Phys. Earth Planet. Interiors 192–193, 1–20.
Von Huene, R., Scholl, D.W., 1991. Observations at convergent margins concerning sediment subduction, subduction erosion, and the growth of continental crust. Rev. Geophys. 29, 279–316.
Williams, G.D., Powell, C.M., Cooper, M.A., 1989. Geometry and kinematics of inversion tectonics. Geol. Soc. Lond 44 (1), 3–15. Special Publications.
Wohletz, K., Civetta, L., Orsi, G., 1999. Thermal evolution of the Phlegraean magmatic system. J. Volcanol. Geotherm. Res. 91, 381–414.
Wyllie, P.J., Huang, W.L., Stern, C.R., Maaloe, S., 1976. Granitic magmas: possible and impossible sources, water contents, and crystallization sequences. Can. J. Earth Sci. 13, 1007–1019.
Wyllie, P.J., 1977. From crucibles through subduction to batholiths. In: Saxena, S.K., Bhattacharjia (Eds.), Energetics of Geological Processes. Springer Verlag, pp. 389–433.